Bactericidal surfaces: An emerging 21st-century ultra-precision manufacturing and materials puzzle ⒻF

Mikel Larrañaga-Altuna, Alaitz Zabala, Iñigo Llavori, Oliver Pearce, Dinh T. Nguyen, Jaume Caro, Holger Mescheder, Jose L Endrino, Gaurav Goel, Wayne Nishio Ayre, Rajkumar Kottayasamy Seenivasagam, Debendra Kumar Tripathy, Joe Armstrong, and Saurav Goel

COLLECTIONS

Ⓕ This paper was selected as Featured

Bactericidal surfaces: An emerging 21st-century ultra-precision manufacturing and materials puzzle (F)

Mikel Larrañaga-Altuna,[1,2] Alaitz Zabala,[2] Iñigo Llavori,[2] Oliver Pearce,[3] Dinh T. Nguyen,[4] Jaume Caro,[5] Holger Mescheder,[6] Jose L Endrino,[7] Gaurav Goel,[1,8] Wayne Nishio Ayre,[9] Rajkumar Kottayasamy Seenivasagam,[10] Debendra Kumar Tripathy,[10] Joe Armstrong,[11] and Saurav Goel[1,8,12,a]

AFFILIATIONS

[1]School of Aerospace, Transport and Manufacturing, Cranfield University, Bedfordshire, MK43 0AL, United Kingdom
[2]Mechanical and Industrial Manufacturing Department, Mondragon Unibertsitatea, Loramendi 4, 20500, Mondragón, Spain
[3]Orthopaedic Department, Milton Keynes University Hospital, MK65 LD, United Kingdom
[4]Multitel ABSL, Rue Pierre et Marie Curie 2, Mons, 7000, Belgium
[5]Eurecat, Centre Tecnològic de Catalunya, Unit of Metallic and Ceramic Materials, Plaça de la Ciència 2, 08243 Manresa, Spain
[6]Fraunhofer-Institut für Produktionstechnologie, IPT, 52074, Aachen, Germany
[7]Nano4Energy SLNE, C/ José Gutiérrez Abascal 2, 28006 Madrid, Spain
[8]School of Engineering, London South Bank University, 103 Borough Road, London, SE1 0AA, United Kingdom
[9]School of Dentistry, Cardiff University, Heath Park, Cardiff, CF14 4XY, Wales
[10]All India Institute of Medical Sciences Rishikesh, India
[11]Polytec GmbH, Polytec-Platz 1–7 76337 Waldbronn, Germany
[12]Department of Mechanical Engineering, Shiv Nadar University, Gautam Budh Nagar, 201314, India

[a])Author to whom all correspondence should be addressed: GoeLs@LSBU.ac.uk

ABSTRACT

Progress made by materials scientists in recent years has greatly helped the field of ultra-precision manufacturing. Ranging from health-care to electronics components, phenomena such as twinning, dislocation nucleation, and high-pressure phase transformation have helped to exploit plasticity across a wide range of metallic and semiconductor materials. One current problem at the forefront of the healthcare sector that can benefit from these advances is that of bacterial infections in implanted prosthetic devices. The treatment of implant infections is often complicated by the growth of bacterial biofilms on implant surfaces, which form a barrier that effectively protects the infecting organisms from host immune defenses and exogenous antibiotics. Further surgery is usually required to disrupt the biofilm, or to remove the implant altogether to permit antibiotics to clear the infection, incurring considerable cost and healthcare burdens. In this review, we focus on elucidating aspects of bactericidal surfaces inspired by the biological world to inform the design of implant surface treatments that will suppress bacterial colonization. Alongside manufacturing and materials related challenges, the review identifies the most promising natural bactericidal surfaces and provides representative models of their structure, highlighting the importance of the critical slope presented by these surfaces. The scalable production of these complex hierarchical structures on freeform metallic implant surfaces has remained a scientific challenge to date and, as identified by this review, is one of the many 21st-century puzzles to be addressed by the field of applied physics.

TABLE OF CONTENTS

NOMENCLATURES

θ	Contact angle
γ_{sv}	Surface tension between the solid phase and vapor phase
γ_{sl}	Surface tension between the solid phase and liquid phase
γ_{lv}	Surface tension between the liquid solid phase
r	Roughness parameter
θ_A	Apparent contact angle
θ_Y	Young's contact angle
f_1	Fraction of solid material in contact with liquid
f_2	Fraction of air in contact with the liquid
θ_1	Contact angle of the solid material
Ø	Diameter
R_a	Arithmetical mean deviation of the assessed profile

Abbreviations

AFM	Atomic Force Microscope
CA	Contact Angle
CAD	Computer-Aided Design
CAH	Contact Angle Hysteresis
CNC	Computer Numerical Control
CVD	Chemical Vapor Deposition
ECAP	Equal Channel Angular Pressing
ED	Emergency department
EDM	Electro Discharge Machining
EDS	Energy-Dispersive Spectroscopy
EPS	Extracellular Polymeric Substance
NHS	National Health Service
PDMSe	Dimethylpolysiloxane
PPI	Plasma Immersion Ion Implantation
SEM	Scanning Electron Microscopy
TEM	Transmission Electron Microscope
UK	United Kingdom
UPM	Ultra-Precision Manufacturing
USA	United States of America

I. INTRODUCTION

Biohazards and biothreats are becoming more ubiquitous than ever before.[1] One of the forefront issues in healthcare is how to avoid repeated surgeries due to implant failure. If one reviews the total life-cycle of an implant, it becomes clear that the challenges faced span fields of materials science[2] (selection of material to avoid stress shielding and ensure biocompatibility), manufacturing (fabrication to obtain the compliant shape by subtractive or additive manufacturing routes), and biological sciences (promoting osseointegration and avoiding biofilm formation and bacterial infection).

Despite processes such as sterilization and even use of antimicrobial coatings, a risk exists of the implant surface being susceptible to bacterial infection at any point of time during its service life. Clinical evidence suggests that numerous species of bacteria are implicated in the infection of medical implants. The most common pathogens identified are *Staphylococcus aureus*,[3] *Escherichia coli*, *Proteus mirabilis*, and *Pseudomonas aeruginosa*.[4] Treating these bacteria with antibiotics alone is often ineffective as *in vivo* they surround themselves awithn active matrix of cells and extracellular substances consisting of glucose[5] (glycocalyx shell) formed on the implant surface, which is impermeable to drugs or antibiotics.[6] As a result, an infected implant usually requires further surgery as part of its treatment. This carries operative and anesthetic risks and a prolonged period of antibiotic treatment thereafter (around 3 months). It is estimated that about 2000 cases of hip and knee replacements become infected every year[7] in the UK alone. Joint replacements are not the only implanted devices in the human body; however, they are one of the most widely studied. Other

implants where infections pose a significant risk include vascular stents, cardiac pacemakers, fracture fixation plates and nails, dental implants, nerve stimulators, cochlear implants, and many more. To address this issue of infection, several different approaches have been proposed: from antibiotic coatings[8] to surface modifications[9] that prevent bacterial adhesion and suppress the proliferation of bacteria.

Nature has become a great inspiration for materials scientists and engineers due to the presence of effective antimicrobial materials with micro and nanostructures, which evolved over millions of years. These hierarchical structures are found mainly in the lotus leaf, gecko skin, dragonfly wings, or cicada wings,[10] among others, giving extraordinary surface properties, such as superhydrophobicity,[11] adhesion,[12] antibiofouling,[13] or bactericidal activity.[14]

Scientists have made collective efforts in order to understand and mimic these extraordinary surfaces, termed nature-inspired surfaces. This is the reason why nature can be considered as the best laboratory for inspiring us to understand hierarchical structures or, put simply, "patterned surfaces." Over the last decade, understanding of micro- and nanometer scale surfaces has played an important role in improving our knowledge of how some of the surfaces seen in nature possess unique properties. For example, it has been reported that the dragonfly wing nanostructure is able to kill either Gram-positive (which have a thick peptidoglycan layer) or Gram-negative (which have a thinner peptidoglycan layer with an additional negatively charged lipopolysaccharide layer) bacteria.[10,15,16] As such, bacterial adhesion has been widely modeled by the Derjaguin, Landau, Verwey, and Overbeek (DLVO) theory, which is governed by van der Waals forces[17] and by various surface properties such as topography, chemical composition, or morphology of the surface,[14,18] which are discussed at length in Sec. III of this paper. Adhesion is also governed by surface conditioning blood proteins, such as fibronectin, fibrinogen, and vitronectin, and other molecules, such as von Willebrand factor and polysaccharides.[5] S. aureus, widely implicated in infection of numerous medical devices, expresses two fibronectin binding proteins (FnBPA and FnBPB), which, as the name suggests, facilitates binding to fibronectin on implant surfaces.[19] Similarly, S. epidermidis, another pathogen associated with joint replacement infections, expresses surface associated autolysin (At1E), which encourages binding to polymeric surfaces.[5] Other mechanisms of adhesion include modulation of fimbriae and polysaccharide adhesins, often associated with Gram-negative bacteria.[20]

The shift from a planktonic (free-floating) to a sessile (attached) state induces expression of several genes responsible for production of extracellular polymeric substance (EPS), resulting in the formation of a biofilm. Both Gram-positive and Gram-negative bacteria can form biofilms on medical devices; most common of which are *Enterococcus faecalis*, *S. aureus*, *S. epidermidis*, and *Streptococcus viridans* (Gram-positive), and *E. coli*, *Klebsiella pneumoniae*, *Proteus mirabilis*, and *P. aeruginosa* (Gram-negative).[21]

Biofilms consist predominantly of a mixture of polysaccharides, nucleic acids (extracellular DNA or eDNA), proteins (composed primarily of D-amino acids), and fatty acids.[22] Extracellular DNA plays a key role in cellular communication in early stages of biofilm development and is modulated by quorum sensing, a density-dependent phenomenon that controls gene expression. *In vivo*, biofilms are often encountered as mixed species with composition of the biofilm varying depending on the species of bacteria present and the properties of the underlying surface. *P. aeruginosa* releases three polysaccharides (alginate, Pel, and Psl) that provide mechanical stability; staphylococci produce polysaccharide intercellular adhesin (PIA) that allows it to form biofilms specifically on orthopedic biomaterials; and more broadly for quorum sensing, Gram-negative bacteria release acyl-homoserine lactones, whereas Gram-positive bacteria release peptide molecules.[22]

The differences in biofilm composition and species present plays an important role in pathogenicity and virulence of the infection. As previously mentioned, staphylococci biofilms are often associated with orthopedic implants, whilst dental implant biofilms consist of a mixed sequential attachment of early colonizers (e.g., *Aggregatibacter actinomycetemcomitans*), followed by bridging species (e.g., *Fusobacterium nucleatum*), and finally more pathogenic bacteria (e.g., *Porphyromonas gingivalis*).[23] Catheter infections are associated with *Proteus mirabilis* biofilms, which results in a rise in pH and subsequent crystallization of minerals and catheter blockage.[24]

Nevertheless, all biofilms follow three classical stages: initial attachment (reversible and irreversible), maturation, and detachment/dispersal, with the main role of the biofilm being to protect the bacteria from the host defense system or from external agents such as antibiotics. It is reported that bacteria in biofilms are 500–5000 times more tolerant toward antibiotics[25] and therefore non-antibiotic approaches to inhibit initial attachment and biofilm formation are clearly needed. By controlling surface properties, the bactericidal efficacy of medical devices such as implants or surgical tools may be improved. Thus, an improved understanding of the bacteria–surface interaction is an important step toward the design of an anti-infective medical implant.

Fabrication of bio-inspired patterned surfaces, however, requires analysis and design of these complex geometries to be reproduced accurately with surface modification methods currently available. An emerging new branch of manufacturing called ultra-precision manufacturing has helped in developing fabrication solutions such as machine tools and processing technologies required for fabricating nanostructured precision surfaces with great repeatability and accuracy. This manuscript is targeted at consolidating a deeper understanding of nature-inspired patterned surfaces and to understand the challenges in fabricating these precise surfaces on somewhat difficult to cut materials, such as CoCr, Ti6Al4V, and stainless-steel alloys, which are among the most popular medical implant materials used.

In this paper, the focus is on salient aspects of "nature-inspired surfaces," primarily applicable to implants. Considering this, some CAD models are proposed according to reviewed literature to facilitate future manufacturing. Moreover, the main surface effects such as topography, wettability, or chemistry are discussed to shed light on how to prevent bacterial adhesion. Finally, the prominent fabrication routes for surface patterning are briefly reviewed. Figure 1 summarizes the structure and content of this interdisciplinary review article.

II. REVIEW OF NATURE-INSPIRED BACTERICIDAL SURFACES

A. Science of wettability

Wetting is the ability of a liquid to maintain contact with a solid surface.[26] Wettability plays an important role in ensuring the desired biological response of biomaterials. Surface wettability may influence adhesion and growth of bacteria on biomaterials and in some cases, it
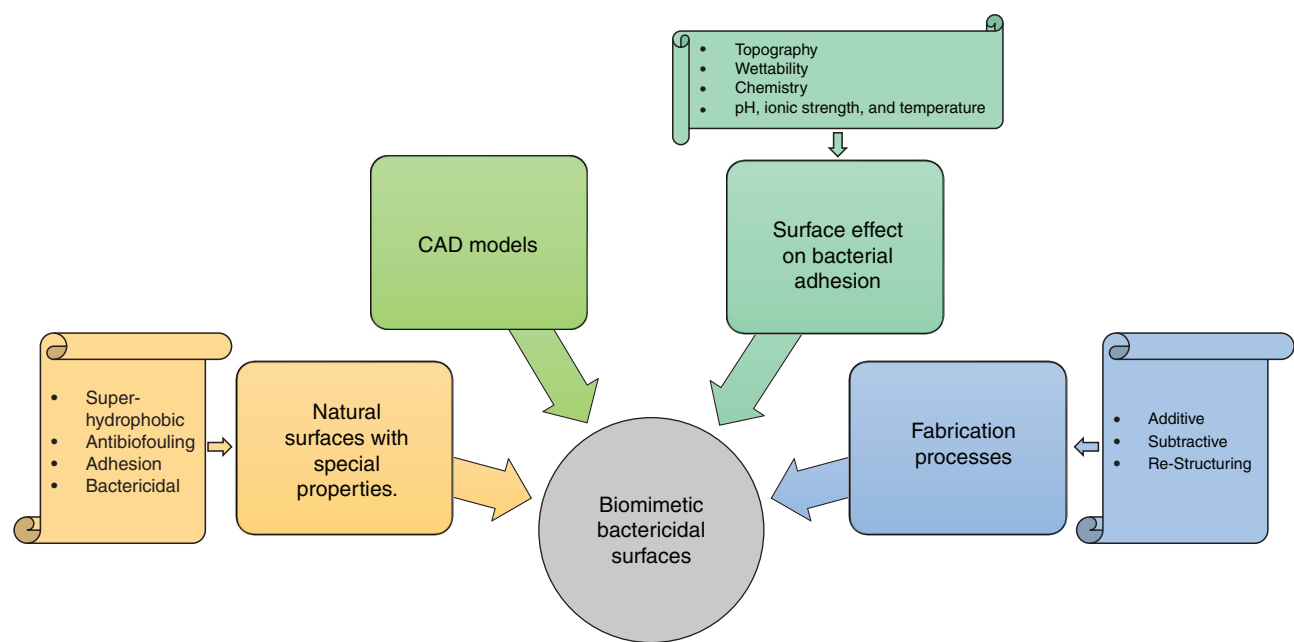
FIG. 1. Schematic representation of the various aspects discussed in this review paper.

is the dominant factor, such as in attachment of *S. epidermidis* on titanium and zirconium dental implants.

Measurement of wettability or in turn the contact angle of a liquid droplet is currently used as an indirect measurement of cellular activity on the surface. However, the exact effect of surface wettability on bacterial adhesion or growth is yet to be established. Wettability is largely governed by surface topography (roughness and morphology) and chemical composition (surface energy).[27] Control of these surface properties has received much interest in a wide range of applications ranging from aerospace, healthcare, and agriculture.[28] Contact angle (θ) is the most widely used indicator to quantify wettability and is determined by calculating the angle between the tangent to liquid-air interface and the line that represents solid-liquid interface. Depending on the contact angle value, a surface may be divided into four main categories[27] as shown in Table I. Different wetting models have been developed to describe the wetting of smooth (Young's) and patterned surfaces (Wenzel's and Cassie-Baxter's equations) as shown in Fig. 2. These models are very important in studying wettability as they can be used for determining contact angles on different surfaces, which in turn defines biological behavior of materials.

TABLE I. Type of surface depending on the CA.

Type of surface	Contact angle (CA)
Superhydrophobic	CA > 150°
Hydrophobic	150° > CA > 90°
Hydrophilic	90° > CA > 10°
Superhydrophilic	CA < 10°

1. Hierarchical structures

Hierarchical structures present a combination of structures at multiple levels (Fig. 3), varying from micro- to nano-level,[29] and can be regarded as composite structures exhibiting features at multiple length scales. They are responsible for non-wetting superhydrophobic properties of natural surfaces, which have been intensively studied as an inspiration for designing and fabricating artificial surfaces used in biomedical applications.[13]

Such surface structures are quite commonly found in plants[30] as well as on animal skin.[31] The most common morphologies found in plants present one convex shape that creates the base at the micrometer level, whereas at the nano-level a cuticular folding is found.[29] The main advantage of these types of structures is that they can create air pockets, leading to the lowest contact area between the surface and water drop, thus presenting an increased contact angle. Figure 4 shows an example of different surface structures and a comparison between contact angles. Koch *et al.*[30] concluded from their investigation that hierarchical structures are responsible for superhydrophobicity in most plants.

2. Young's model of wettability

Young's model is used to describe wetting on ideally smooth, rigid, chemically homogeneous, insoluble, and non-reactive surfaces.[14] On these surfaces, the contact angle (θ) depends on surface free energy and is calculated as

$$\cos \theta = \frac{\gamma_{sv} - \gamma_{sl}}{\gamma_{lv}}, \qquad (1)$$

where θ is Young's contact angle, γ_{sv} is surface tension between solid phase and vapor phase, γ_{sl} between solid phase and liquid phase, and γ_{lv} between liquid solid phase.
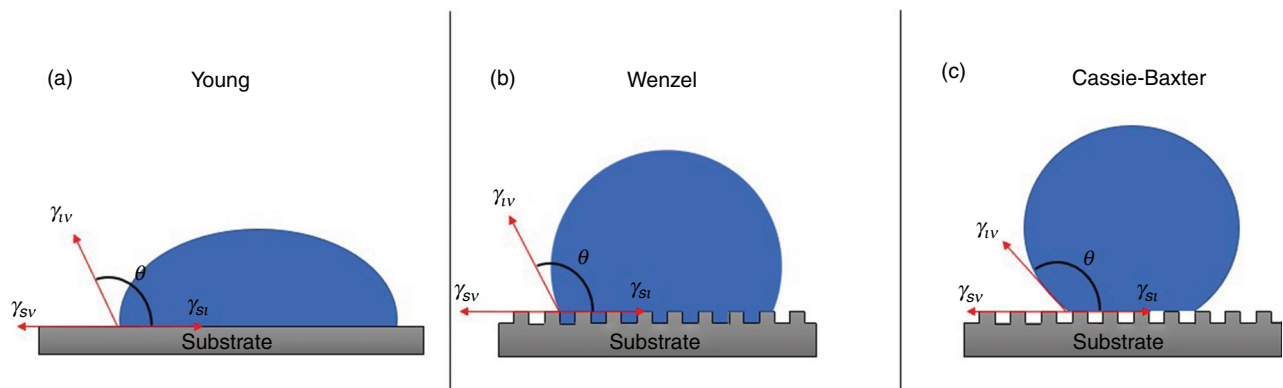
FIG. 2. Models used to measure the contact angle of the surface. (a) Young, (b) Wenzel, and (c) Cassie-Baxter model.
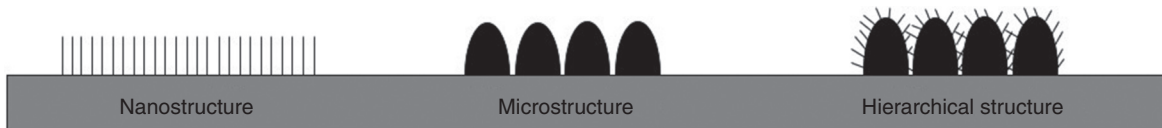
FIG. 3. Different levels of structures, from nanostructures to hierarchical structures.

The Young's Eq. (1) is only valid for a flat and homogeneous surface with Young's contact angle smaller than 120°. When surfaces are not considered ideally smooth, rigid, or chemically homogeneous, Young's models cannot be employed. For rough surfaces, two different models have been developed to better describe the wettability about surface roughness and surface energy, and these are Wenzel and Cassie-Baxter models [shown in Fig. 2(b) and Fig. 2(c)], respectively.

3. Wenzel model of wettability

The Wenzel model describes the homogeneous wetting regime of textured surfaces.[32] It means that a water drop sits on the surface, wetting the whole area [Fig. 2(b)]. The contact angle for this case can be estimated as[33]

$$\cos \theta_A = r \cos \theta_Y, \tag{2}$$

where θ_A is the apparent contact angle, θ_Y is Young's contact angle, and r is the roughness parameter, defined as projected area of the water droplet.[14] The Wenzel model [Eq. (2)] shows that for a rough surface, the apparent contact angle increases with increased surface roughness. However, this relationship only holds with a surface roughness smaller or equal to 1.7 μm ($r \leq 1.7$). If greater than that, the heterogeneous regime (described by Cassie-Baxter's model) starts, in which air is increasingly presented and trapped between solid and water surfaces, resulting in a decrease in this angle.

4. Cassie-Baxter model of wettability

The Cassie-Baxter model describes the heterogeneous regime where the water drop does not wet the whole surface due to air
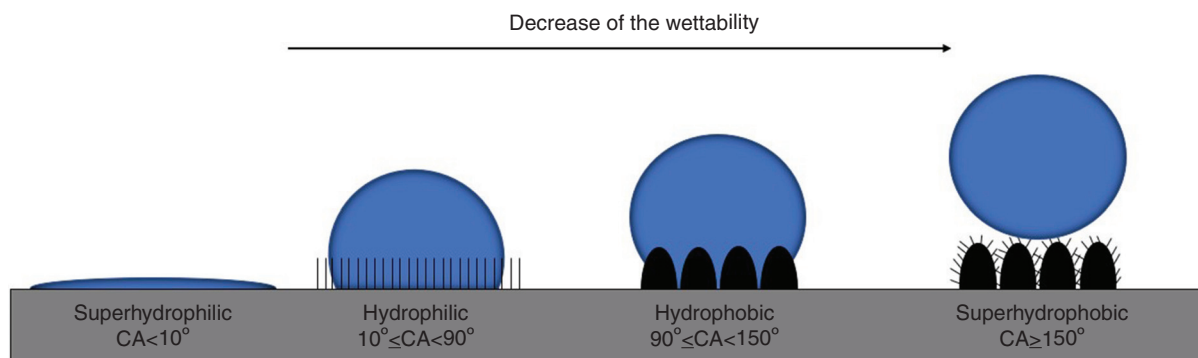
FIG. 4. Different surface structures, starting smooth surface (left), nanostructure, microstructure, and hierarchical structure (right). Reproduced with permission from K. Koch, B. Bhushan, and W. Barthlott, J. Soft Matter **4**, 1943 (2008), Copyright 2008, Royal Society of Chemistry.[30]
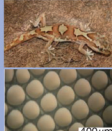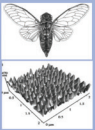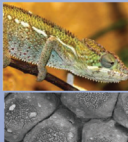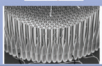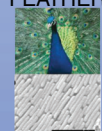
FIG. 5. Functionalities of some of the nature-inspired surfaces and some of their most studied properties.

trapped between the rough surfaces [Fig. 2(c)]. For this model, contact angle[34] may be calculated as

$$\cos \theta_A = f_1 \cos \theta_1 - f_2, \qquad (3)$$

where θ_A is the apparent contact angle, θ_1 is contact angle of solid material, f_1 is fraction of solid material in contact with fluid, and f_2 is fraction of air in contact with liquid. The droplets in the Cassie-Baxter model provide a higher contact angle due to air trapped between the surface and water drop.[35] Carbone et al.[36] reported an analytical model where the transition from the Cassie-Baxter and Wenzel model has been calculated for rough surfaces taking into account the applied pressure and height of the rough surface.

B. Functionalities of selective nature-inspired patterned surfaces

A wide range of natural surface functionalities has attracted scientists over the last few decades due to their special properties. Sun and Bhushan[37] gathered the most studied natural surfaces over the last 45 years, starting from the superhydrophobic shark skin property discovered in 1985 to the drag reduction property discovered in 2016. Figure 5 shows a few examples of natural functionalities and the most studied examples.

1. Superhydrophobicity

The lotus leaf is known for its self-cleaning and superhydrophobic properties.[13,38–40] This extraordinary property relies on its randomly distributed 5 to 9 μm diameter micropapillae covered by branch-like nanostructures 120 nm in diameter and 200 to 400 nm long,[11,31,41] shown in Fig. 6.

It should be noted that the lotus leaf microstructure is covered by epicuticular waxes (made from hydrocarbon chains). The combination of hierarchical structure and the waxes lead to improved contact angle of up to 164°.[42] Nishimoto et al.[39] reported that if the superficial waxes are removed with acetone, the CA decreases dramatically, which
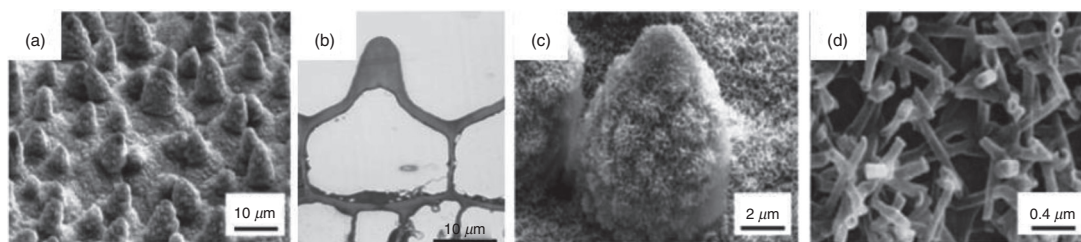
FIG. 6. (a) Microstructure of lotus leaf. Reproduced with permission from K. Koch, B. Bhushan, Y. C. Jung, and W. Barthlott, J. Soft Matter **5**, 1386 (2009), Copyright 2009, Royal Society of Chemistry.[42] (b) Cross section of micropapillae. Reproduced with permission from H. J. Ensikat, P. Ditsche-Kuru, C. Neinhuis, and W. Barthlott, Beilstein J. Nanotechnol. **2**, 152 (2011), licensed under a Creative Commons Attribution (CC BY) license.[43] (c) Micropapillae covered with epicuticular waxes and d) branch-like nanostructures. Reproduced with permission from K. Koch, B. Bhushan, Y. C. Jung, and W. Barthlott, J. Soft Matter **5**, 1386 (2009), Copyright 2009, Royal Society of Chemistry.[42]
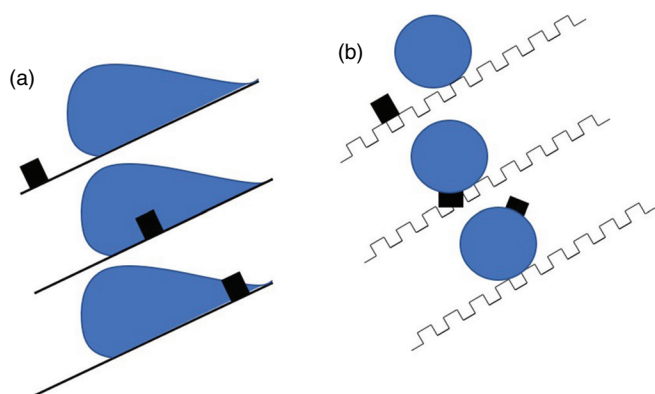
FIG. 7. Schematic illustration of the lotus leaf self-cleaning effect (a) ideal smooth surfaces and (b) rough surfaces (black mark indicates a roll-off point).

FIG. 9. (a) Butterfly wing scales, scale bar 100 μm and (b) nanostripes, scale bar 100 nm. Reproduced with permission from Y. Zheng, X. Gao, and L. Jiang, J. Soft Matter **3**, 178 (2007), Copyright 2007, Royal Society of Chemistry.[53]

highlights the importance of surface chemistry alongside surface geometry. Besides, a lotus leaf has a Contact Angle Hysteresis (CAH) of less than 5°.[39] For lower values of CAH, the droplet may roll and slide on the surface.[44] The combination of superhydrophobicity and low CAH provides a self-cleaning effect for the lotus leaf (Fig. 7).

These properties make the lotus leaf an ideal bacterial repellent surface.[45] Fadeeva *et al.*[46] used laser processing to mimic the lotus leaf hierarchical structures on titanium. They reported a significant reduction in Gram-negative *P. aeruginosa* bacteria in comparison to a polished surface. In contrast to this, an increase in Gram-positive *S. aureus* bacterial adhesion was observed. Similar structures may be seen on the taro leaf, possessing superhydrophobicity and self-cleaning abilities due to hierarchical structure.[47] The microstructure of this surface consists of elliptical bumps, 10 to 30 μm in diameter, covered by randomly distributed epicuticular waxes (Fig. 8). Similar to a lotus leaf, these waxes increase the contact angle of taro leaf from 90° to 150°.[45]

Another example of a superhydrophobic surface is found on the *Morpho aega* butterfly wing.[31,48–52] The wings are not only superhydrophobic (CA of 152 ± 2°[39]) but also attractive to insects due to their chemical sensing capability or physical fluorescence emission functions.[39] The microstructure of these wings consists of overlapped scales, 150 μm in length and 70 μm in width, where each scale consists of ridging nanostripes 184 nm in width with a

585 nm clearance.[53] Figure 9 shows the microstructure of *Morpho aega* butterfly wings.

2. Anti-biofouling

Shark skin is known to possess anti-biofouling, self-cleaning, hydrophobic, and hydrodynamic properties evolved over millions of years.[44] These properties rely on a rhombus denticle based microstructures with five riblets 200 to 300 μm in length, 20 to 30 μm in height, and 50 to 80 μm in width. Figure 10 shows a representation of shark skin microstructure, which helps a shark to swim fast.[54]

Due to these outstanding properties, different attempts have been carried out to mimic shark skin. Chung *et al.*[55] manufactured a PDMSe elastomer with Sharklet AF^{TM} microstructure (Fig. 11). Sharklet AF^{TM} is known as the most successful design to replicate shark skin.[56,57] In their study, *S. aureus* bacteria was employed to test the bactericidal efficacy of this surface. After 31 days, the results showed a 42% less covered bacterial area on the structured surface compared to a smooth surface. Furthermore, no biofilm formation was observed on the Sharklet AF^{TM} surface.

3. Adhesion

Lots of insects and animals, such as flies, bees, and geckos, are well known for their ability to stick onto a wide range of surfaces. Geckos are a particularly interesting species because of high body mass and high density of terminal elements.[31] The detachment mechanism
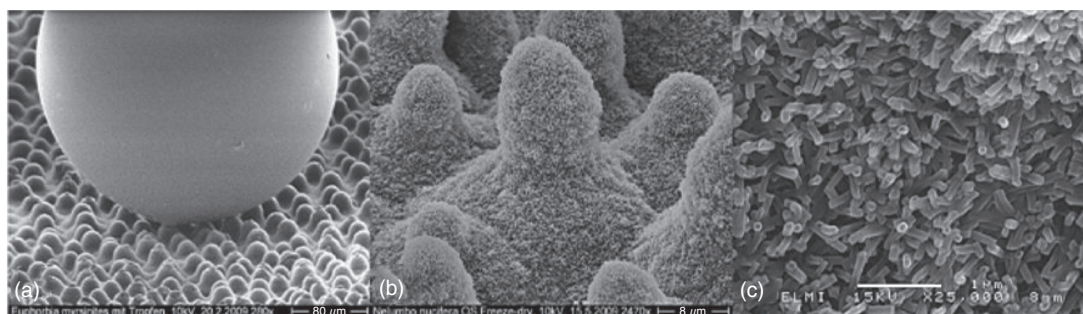
FIG. 8. (a) SEM image of the taro leaf with a water droplet showing the superhydrophobic properties. (b) Taro leaf bump-like microstructure and (c) bumps covered by epicuticular waxes. Scale bars are (a) 80 μm (b) 8 μm (c) 1 μm. Reproduced with permission from Y. Y. Yan, N. Gao, and W. Barthlott, Adv. Colloid Interface Sci. **169**, 80 (2011), Copyright 2011, Elsevier.[47]

FIG. 11. Scanning electron micrograph of the top view of Sharklet AF™ microstructure. Reproduced from K. K. Chung, J. F. Schumacher, E. M. Sampson, R. A. Burne, P. J. Antonelli, and A. B. Brennan, BioInterphases **2**, 89 (2007), with the permission of AIP Publishing.[55]

FIG. 10. Shark skin riblet based microstructure. Scale bar 100 μm. Reproduced with permission from D. Y. Zhao, Z. P. Huang, M. J. Wang, T. Wang, and Y. Jin, Mat Proc. Tech. **212**, 198 (2012), Copyright 2012, Elsevier.[54]

of micropatterned natural surfaces (geckos included) has been widely studied.[58]

The hierarchical structure of the gecko foot consists of hundreds of setae varying from 30 to 130 μm long with each seta having hundreds of spatulae in sizes from 0.2 to 0.5 μm[31,59] Figure 12 shows details of the gecko's foot microstructure.

It has been reported that gecko feet can generate a 10 N adhesive force per 10 mm^2 area.[31] Spatulae can tolerate higher load (several times the weight of the geckos) by van der Waals forces.

The gecko's foot is not the only scientifically attractive part of this animal; the dorsal or abdominal parts (Fig. 13) also possess some

advanced surface properties such as antibacterial or self-cleaning[12,61] characteristics. The hierarchical structure of the gecko's abdomen consists of 100 to 190 μm diameter scales (up to 300 μm for dorsal), 50 μm in height [Fig. 13(c)]. Each scale is covered with hundreds of spinules, the length of which varies from 0.5 to 1 μm with a 10 to 30 nm radius of curvature at their tip [Fig. 13(e)].

Regarding the antibacterial and self-cleaning properties of the gecko dorsal and abdominal dorsum, Watson *et al.*[12] carried out bacterial and self-cleaning experiments where gecko dorsal skin was analyzed. For the bacterial analysis, *P. gingivalis* bacteria (associated with dental implant infections) were employed, and for the self-cleaning ability, water droplets were employed. They concluded that the gecko dorsal skin CA was between 151° and 155° and was able to decrease *P. gingivalis* adhesion as well as having a self-cleaning ability. Li *et al.*[62] also compared the adhesion of two different bacteria into the dorsal dorsum of the gecko. They proposed a model for the interaction between Gram-negative bacteria and the gecko skin. A mechanism that, due to the stretching and compression between the bacteria and gecko spinules, causes bacterial rupture.

4. Bactericidal surfaces

Bactericidal surfaces are bacterial resistant surfaces capable of eliminating bacteria by providing reduced contact area to thereby create tensile strain in the cell walls of the bacteria causing it to rupture. There are many bactericidal surfaces reported, such as those of the
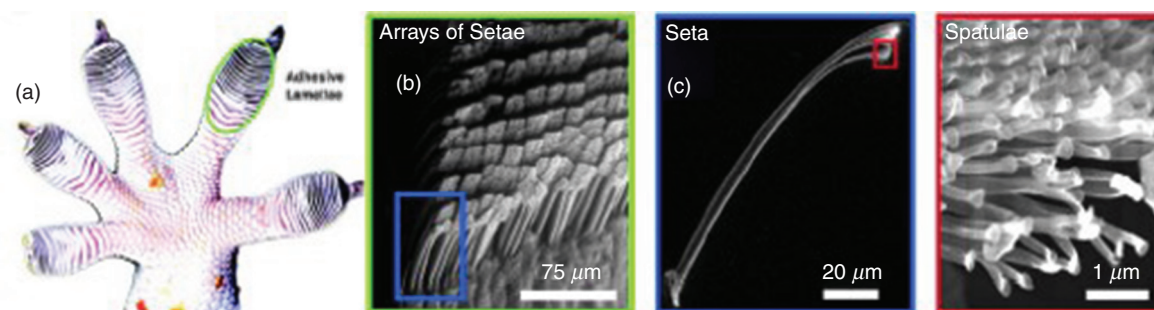
FIG. 12. (a) Gecko foot. (b) Group of setae, (c) a single seta, and (d) group of spatulae. Reproduced with permission from W. R. Hansen and K. Autumn, Prog. Nat. Acad. Sci., **102**, 385 (2005), Copyright 2005, US National Academy of Sciences.[60]
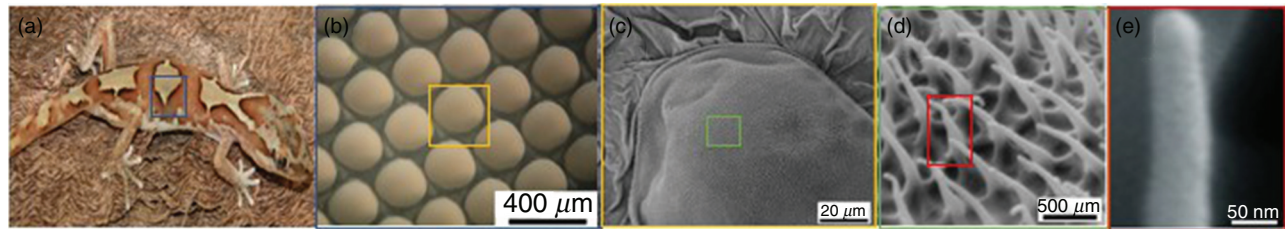
FIG. 13. (a) *Lucasium steindachneri* gecko. (b) Optical image of the abdominal part of gecko. (c) Topographical SEM image of the scales. (d) Group of spinules in the top of the scales. (e) Magnification of the spinules at the nanometer scale. Reproduced with permission from G. S. Watson, D. W. Green, L. Schwarzkopf, X. Li, B. W. Cribb, S. Myhra, and J. A. Watson, Acta BioMaterialia **21**, 109 (2015), Copyright 2015, Elsevier.[12]

lotus leaf or gecko skin that, due to the anti-biofouling or self-cleaning properties, may avoid the growth of bacterial adhesion.[10,38,39,45] Some insect wings have been investigated due to their bactericidal properties, such as cicada and dragonfly wings, which showed great promise for developing anti-infective surfaces.[10,38,45]

Cicada wings are known to be bactericidal against *P. aeruginosa* and *S. cerevisiae*.[10,38,63] The nanostructure of the cicada wing consists of nanopillars with 200 nm height, 170 nm spacing, and 60 and 100 nm top and base diameters, respectively.[63] Figure 14(a) shows an Atomic Force Microscope (AFM) image of the cicada wing nanostructure. Moreover, apart from being bactericidal surfaces, they are also known for superhydrophobicity, with CA of 160° and self-cleaning properties.[10]

It should be noted that the anti-biofouling property of cicada wings does not lie in the ability to repel the bacteria, but in its surface nanostructure and ability to kill the bacteria by contact.[10]

It was reported that the cicada wings were able to kill only Gram-negative bacteria.[65] This was attributed to the wall thickness of a Gram-negative bacteria, which is 4 or 5 times thinner than Gram-positive bacteria.[10] Ivanova *et al.*[63] carried out an experiment where *P. aeruginosa* bacteria were tested on the Cicada wings. It was observed that this surface was able to effectively kill this bacterium.

To advance the understanding of the interaction between Gram-negative bacteria and the cicada wing surface nanostructure, Pogodin *et al.*[66] developed a biophysical model. They concluded that the region where the bacteria ruptured was between the pillars (Fig. 15). Specifically, it was not the intrusion of the structure into the substance of the bacterium that punctures the bacterium, but a rupture of the membrane in the region between adjacent spikes. Rupture of the bacterial membrane results in catastrophic leakage of the cellular contents resulting in bacterial death.

A recent study by Román-Kustas *et al.*[67] shows that the bactericidal effect of the cicada wings is not only attributed to the surface morphology, but the chemical composition of the surface also plays a key role in the bacterial rupture.

Another natural excellent bactericidal surface is found on dragonfly wings.[45] This surface has a CA of 153°[10]. The nanostructure of the dragonfly wing consists of randomly distributed nanopillars with a variable diameter between 50 and 80 nm, 200 to 300 nm in height, and 180 nm spacings between the pillars (Fig. 16).[68] In contrast to this, Bandara *et al.*[15] analyzed the topography of the dragonfly wing and identified two pillar type structures: randomly distributed tall and short nanopillars. They reported a base diameter of 37 ± 6 nm and 57 ± 8 nm for short and tall nanopillars, respectively, and 189 ± 67 nm and 311 ± 52 nm height for short and tall, respectively.

It has been proven that the bactericidal efficacy lies in the nanostructure both for the dragonfly wings as well as cicada wings.[68] Despite this, a great advantage of dragonfly wings over the cicada
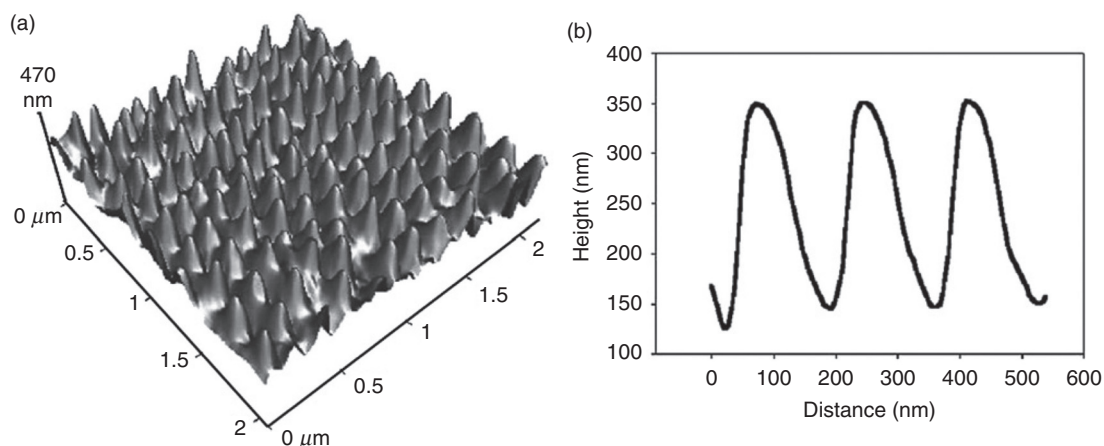
FIG. 14. (a) AFM three-dimensional image of a cicada wing and (b) corresponding height and width profile. Reproduced with permission from G. S. Watson, S. Myhra, B. W. Cribb, and J. A. Watson, J. of BioPhysics **94**, 3352 (2008), Copyright 2008, Elsevier.[64]
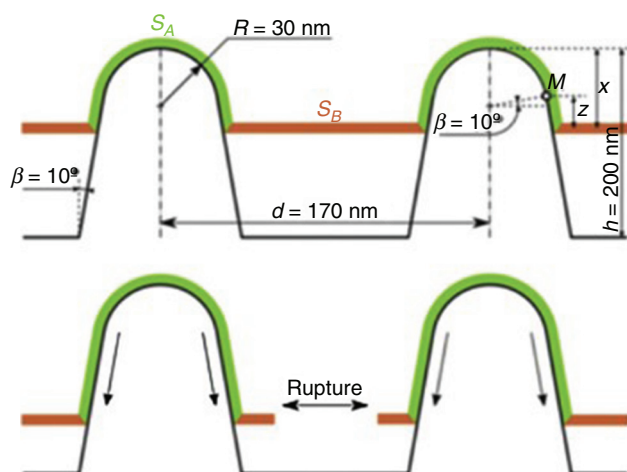
FIG. 15. Model of cicada wing and bacteria explaining rupture of bacteria. Reproduced with permission from S. Pogodin, J. Hasan, V. A. Baulin, H. K. Webb, V. K. Truong, T. H. Phong Nguyen, V. Boshkovikj, C. J. Fluke, G. S. Watson, J. A. Watson, R. J. Crawford, and E. P. Ivanova, J. of BioPhysics **104**, 835 (2013), Copyright 2013, Elsevier.[66]

FIG. 16. Pillar-like nanostructure of the dragonfly wings. Reproduced with permission from C. D. Bandara, S. Singh, I. O. Afara, A. Wolff, T. Tesfamichael, K. Ostrikov, and A. Oloyede, ACS Applied Materials and Interfaces **9**, 6746 (2017), Copyright 2017, American Chemical Society.[15]

wings is its ability to kill both Gram-positive and Gram-negative bacteria.[45]

Bhadara *et al.*[69] were inspired by the dragonfly wing and attempted to mimic its topography on titanium surfaces. Hydrothermal etching processes were employed, and *P. aeruginosa* and *S. aureus* adhesion was tested. An increase in the CA and reduction in the bacterial attachment was observed for both samples compared to the non-treated titanium. Although the decrease in bacterial adhesion was observed for both cases, significantly more non-viable *P. aeruginosa* were observed.

Modaresifar *et al.*[70] gathered the currently available evidence to show how different nanopatterned surfaces influence bacterial adhesion. The authors reviewed around 46 studies to conclude that the most common heights are between 100 and 1000 nm with a diameter in the range of 10 to 300 nm and less than 500 nm spacings. They also concluded that the most common structures that avoid bacterial adhesion were nanopillar-based structures.

5. Optical adjustment

Optical adjustment is the ability of animals and plants to adapt and change their skin color according to the environment. The most well-known example is the chameleon, which appears to change its skin color to increase survival chances.[71] These color-changing properties lie in its skin cells, called chromatophores.[72] These chromatophores have a mixture of blue, white, red, and yellow pigments, so with the correct combination of pigments, the chameleon can adjust its skin to a wide range of colors depending on the environment. The microstructure of chameleon skin consists of scales that can vary in size between a few micrometers or millimeters [Fig. 17(a)], which are covered by setae ranging from 10 to 30 μm [Fig. 17(c)].[73] Several attempts have been made to replicate the chameleon skin for different applications.[74–76]

Moreover, some species of brittle stars (*Ophiocoma wendtii*) showed a color-changing ability, from dark brown in the day to gray and black at night (Fig. 18).[77,78] This reaction is due to dermal receptors that consist of single crystal-oriented calcite (10–15 μm).[31,78]

6. Sensing to stimulus

Some leaves such as of *Mimosa pudica* plants are extremely sensitive to physical contact, they may open [Fig. 19(a)] and close [Fig. 19(b)] on being touched.[79]

FIG. 17. Scanning electron micrographs of the *Chameleo calyptratus*. (a) Microstructure of the chameleon skin with a scale-like microstructure. (b) Setae covering the scale-like microstructure. (c) Cross-section of the scale with the setae (S). Reproduced with permission from M. Spinner, G. Westhoff, and S. N. Gorb, Sci. Report **4**, 1 (2014), Copyright 2014, Springer Nature.[73]

FIG. 18. (a) Brittle star image and (b) SEM image of its microstructure. Reproduced with permission from J. Aizenberg, A. Tkachenko, S. Weiner, L. Addadi, and G. Hendler, Nature **412** (2001), Copyright 2001, Springer Nature.[78]

This extraordinary property lies on its base where the pulvini are placed. The pulvini at the same time store the mechanical and photo-receptors that enable them to open and close.[80] Moreover, the leaves of these plants can open in the night or day.[81]

7. Hard and tough surfaces

The main challenge for the human tooth is to be able to withstand constant loads and stresses without fracturing. They are natural tissues with excellent mechanical properties due to their hierarchical structures.[82,83] This hierarchical structure consists of an outer layer called the enamel, an intermediate dentin layer and the pulp (the core), see Fig. 20.[44]

On one hand, the enamel is the hardest tissue type and is the one that offers continuous mechanical and chemical resistance.[84,85] On the other hand, dentin consists of small cylindrical tubes (1 to 3 μm diameter) surrounded by hydroxyapatite and organic elements. Dentin offers elasticity and mechanical strength to the teeth.

8. Optics

The colors of animals or plants are created by pigmentation, changing the angle of view (iridescence), by architecture, or a combination of the above. It is believed that those that change color as a result of architectural changes do so because of the interaction of light and the hierarchical structures.[86] The *Morpho aega* butterfly wings, apart from exhibiting superhydrophobic properties, also exhibit blue iridescent colors (different colors if the angle of view is changed).[87–89]

Another example of this is the peacock feather (Fig. 21).[90] The range of colors that appear on its feathers is due to the 2D photonic crystal structure.[91] The microstructure consists of 184 nm diameter
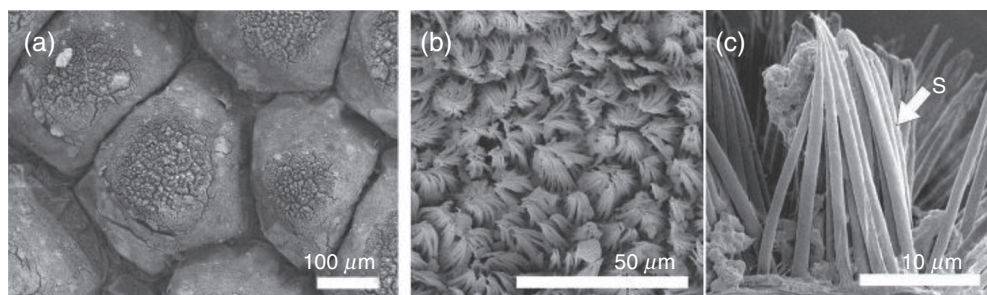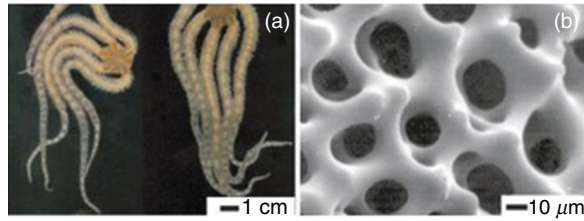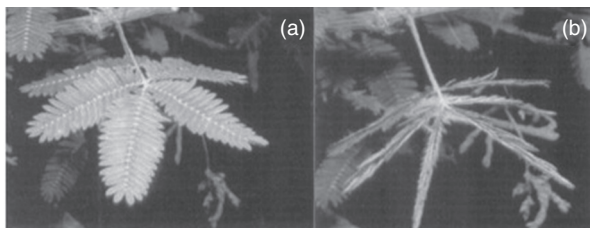

FIG. 19. Leaves of the *Mimosa pudica* (a) open and (b) closed. Reproduced with permission from H. S. Patil and S. Vaijapurkar, J. Bionic Eng. **4**, 19 (2007), Copyright 2007, Springer.[80]

and 3 to 14 μm length nanofibers, where the space between the fibers are filled with air.[92]

C. Bactericidal CAD models inspired by nature

Bacterial infection on surgical implants remains a formidable problem. Table II gathers the reported dimensions of the most promising antibacterial and bactericidal surfaces (in cases where the dimension was not explicitly reported, they were extracted using image processing).

On the other hand, Table III shows a summary of some mimicked antibacterial surfaces in terms of their dimensions and obtained outcomes.

Manufacturing of bactericidal surfaces requires good design and modeling of those structures to be developed. In this section, some bactericidal CAD models are proposed. More detailed information related to the dimensions of each structure is shown in Table IV.

As previously mentioned, the lotus leaf presents antibacterial properties due to its outstanding superhydrophobicity. Figure 22 depicts the lotus leaf surface structure and the proposed CAD model.

The nanostructure of cicada wings is bactericidal against Gram-negative bacteria. Figure 23 shows the model created to mimic cicada wings.

Also, dragonfly wings possess excellent bactericidal efficacy against Gram-positive and Gram-negative bacteria. It is believed that this extraordinary property is due to the nanopillar-based nanostructures. With this structure, nanopillars can damage the bacterial wall, leading to its rupture. Figure 24 shows a model made for this nanostructure.

The shark skin has been proven to be antibacterial due to its anti-biofouling and self-cleaning properties.[105] It is documented that the most accurate reproduction of shark skin has been made by Sharklet AF^{TM}.[55] Figure 25 shows a representative model of Shark skin.

This model consists of grooves with length varying from 4 to 16 μm, the height is 3 μm, and the spacing between the grooves is 2 μm.

Moreover, Mann et al.[107] carried out a clinical study (simulation) where they used shark skin based micropatterned surfaces compared to an un-patterned surface. They observed a reduction of attached *S. aureus* but not complete abolition. Finally, Fig. 26 shows the model for the Gecko animal skin.

The challenge of mimicking a natural surface lies both in the understanding of the multiscalar patterned hierarchical structures (see Table IV) as well as in the scalable fabrication of freeform surfaces. The next focus in Sec. III is to unravel the current understanding of the root causes of bactericidal properties, and then Sec. IV discusses the cutting-edge manufacturing methods to shed some light on the various possibilities and limitations of these methods.

III. BACTERICIDAL EFFECT ON SURFACE PROPERTIES

Several attempts are made to model the bacteria-surface interactions and to understand bacterial adhesion with a surface. In this section, some important surface properties contributing to the observed bactericidal effect are presented and discussed. Figure 27 shows the representation of the bactericidal effect of surface properties.
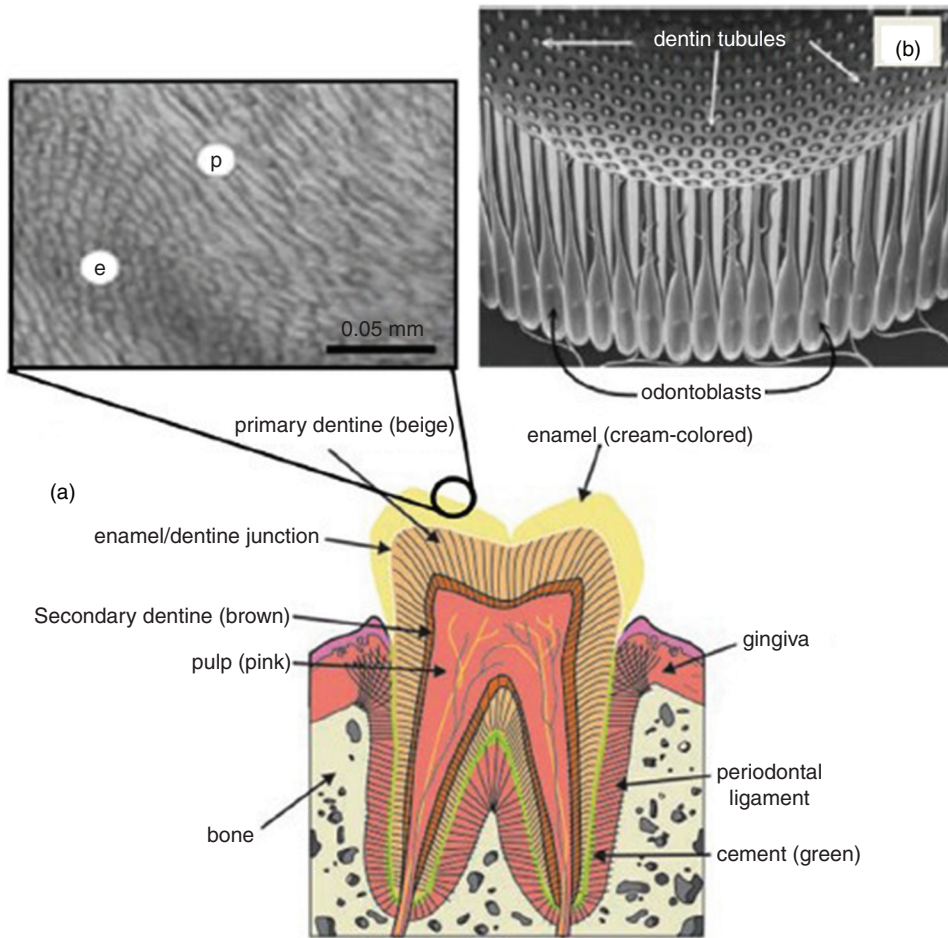
FIG. 20. (a) The main structure of human teeth. (b) Tubular structure of dentin. Reproduced with permission from A. Malshe, K. Rajurkar, A. Samant, H. N. Hansen, S. Bapat, and W. Jiang, CIRP J. Mfg. Tech. **62**, 607 (2013), Copyright 2013, Elsevier.[31]

A. Topography: Roughness and shape

Several studies have tried to establish the relationship between surface roughness and bacterial adhesion.[108] Truong *et al.*[109] performed a study where *S. aureus* and *P. aeruginosa* were tested on titanium grade 2 samples with a surface treatment based on equal channel angular pressing (ECAP). The surface roughness R_a (for an
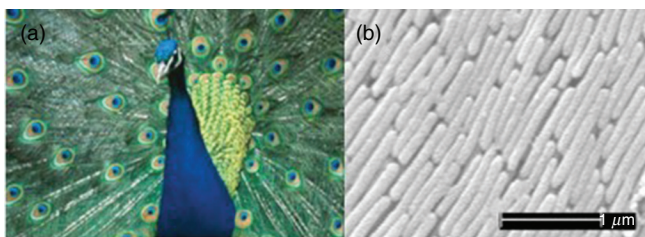
FIG. 21. (a) Peacock with its feathers. Reproduced with permission from S. C. Burgess, A. King, and R. Hyde, Optics and Laser Technology **38**, 329 (2006), Copyright 2006, Elsevier.[90] (b) Longitudinal cross section of the barbs. Reproduced with permission from J. Zi, X. Yu, Y. Li, X. Hu, C. Xu, X. Wang, X. Liu, and R. Fu, Prog Nat Acad Sci, **100**, 12576 (2003), Copyright 2003, US National Academy of Sciences.[91]

AFM measure of 40 μm × 40 μm) of the samples were 2.90 ± 1.74 μm and 3.80 ± 1.39 μm for the unprocessed and processed samples, respectively. They concluded that the bacteria preferentially adhered to the modified surface due to the increasing contact area at the nanometer scale.

Ivanova *et al.*[110] studied the attraction and repulsion effect of *S. aureus* and *P. aeruginosa* on different titanium thicknesses. It was observed that *S. aureus* were more adherent to the same surface roughness than *P. aeruginosa*. They concluded that *P. aeruginosa* attached on surfaces with an R_a value below 0.5 nm whereas *S. aureus* attached on surfaces with an R_a value between 3 and 12 nm. It was also suggested that cell morphology could be one of the reasons why bacteria exhibit different adhesion properties. Aykent *et al.*[111] carried out experiments where different materials with different surface finishes were tested against *S. mutans*. It was observed that for the same materials, a decrease in the bacterial adhesion was observed if the surface roughness decreased.

Moreover, Taylor *et al.*[112] studied the influence of the surface roughness on *S. aureus* and *P. aeruginosa* bacterial adhesion. The R_a was varied from 0.04 to 7.89 μm, but despite the difference in the surface roughness, similar bacterial adhesion was found both on smooth and rough surfaces. They suggested that the bacterial adhesion was

TABLE II. Natural dimensions of most promising antibacterial surfaces based on the literature.

Natural surface	Wettability (°)	Microstructure			Nanostructure			Reference
		Height (μm)	Base (μm)	Spacing (μm)	Height (nm)	Base (nm)	Spacing (nm)	
Lotus leaf	>150	-	Ø5-Ø9	-	-	Ø120	-	31
Lotus leaf	164	13	Ø10	-	780	Ø400	-	13
Lotus leaf	>150	10.4 ± 0.8	8 ± 2.4	19.5 ± 12.5	530 ± 150	Ø100 ± 30	-	93
Shark skin	-	200-500	100-300	100-300	-			44
Shark skin	-	8	-	60	-			94
Gecko dorsal	151-155	50	Ø100-Ø190	50	Up to 4000	-	-	12
Gecko dorsal	-	-	160	210	3000	Ø350-Ø400	500	95
Cicada wing	144 ± 7		Not hierarchical		200	Ø170	200	64
Cicada wing	-		Not hierarchical		300	Ø90	170	96
Cicada wing	146		Not hierarchical		146-157	Ø82-148	44-177	45
Cicada wing	159		Not hierarchical		200	Ø60 top and Ø100 base	170	63
Dragonfly wings	-		Not hierarchical		350	Ø80	150	96
Dragonfly wings	153		Not hierarchical		240	50-70	200	97
Dragonfly wings	-		Not hierarchical		Small: 189 ± 67 Tall: 311 ± 52	Small: 37 ± 6 Tall: 57 ± 8	-	15
Dragonfly wings	-		Not hierarchical		79.63-188.31	Ø83.25-Ø195.08	-	98
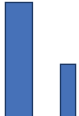
TABLE III. Some bio-mimicked antibacterial surfaces and obtained outcomes.

Bio-inspiration	Fabrication process	Material	Surface type	Dimensions	Bactericidal effect	Reference
Dragonfly wing	Hydrothermal etching	Titanium	Nanowires	Ø40.2 ± 20 nm	*P. aeruginosa*: 50% death. *S. aureus*: 20% death	69
Dragonfly wings	Reactive ion etching and CVD	Black silicon	Nanopillars	Ø20 nm–Ø80 nm Spacing: 200 nm–1800 nm	Effective against Gram positive and Gram-negative bacteria.	97
Dragonfly wings	Ion etching	Silicon	Nanopillars	Ø220 nm and 4 μm height	83% of Gram negative (*E. coli*) and 86% of Gram positive (*S. aureus*) bacteria were killed	99
Cicada wing	Hydrothermal method	TiO$_2$	Nanowires	Ø100 nm and Ø10 μm–15 μm Heights: 3 μm	*P. aeruginosa*: More than 50% death *S. aureus*: Less than 5% death	100
Cicada wing	Glancing angle sputter deposition	TiO$_2$ on silicon substrate	Nanopillars	Ø33 ± 7 nm Peak-peak: 158 ± 105 nm	*E. coli*: 50% death *S. aureus*: Successfully colonized.	101
Cicada wing	Nanoimprinting lithography	PMMA	Nanopillars	Ø150 nm, 400 nm height and 150 nm spacing	-	102
Cicada wing	Thermal oxidation	Ti6Al4V	Nanospikes	Ø20 nm	Enhance the bactericidal activity against *E. coli*	103
Lotus leaf	Femtosecond laser	Titanium	Microbumps	Ø10 μm–Ø20 μm	Lower adhesion of *P.*	46

TABLE III. (*Continued.*)

Bio-inspiration	Fabrication process	Material	Surface type	Dimensions	Bactericidal effect	Reference
				grains and 200 nm undulations	*aeruginosa* than polishes but increase of *S. aureus*.	
Lotus leaf	Femtosecond laser	Titanium	Microbumps	Ø10 μm–Ø20 μm grains and 200 nm undulations	*S. aureus, S. epidermidis* and *P. maritimus* were able to attach to the surface.	104
Gecko skin	Template process	Epoxy resin	Nanoairs	2 μm–4 μm length 2 μm height 500 nm spacing and base	*S. mutans:* First 3 days lower adhesion than original skin. After 7 days more than natural skin	62
					P. gingivalis: Higher adhesion than natural skin.	
Shark skin	Photolithography + ion etching	PDMSe	Grooves	2 μm width and spacing 3 μm height	Decrease of bacterial adhesion than smooth surface and avoid of biofilm formation.	55

TABLE IV. Summary of the modeled bioinspired bactericidal structures dimensions.

Natural surface	Microstructure			Nanostructure			Slope
	Height (μm)	Width (μm)	Spacing (μm)	Height (nm)	Width (nm)	Spacing (nm)	
Lotus leaf	10	Ø8	14	400	Ø200	150	
Cicada wing		Not hierarchical structures		200	Base: Ø100 Top: Ø60	110	
Dragonfly wing				Small: 189 Tall: 311	Small: Ø37 Tall: Ø57	Small. 170 Tall: 1943	
Shark skin	3	2 × 4–8-12–16	2		Not hierarchical structure		
Gecko skin	50	Ø150	170	700	Ø200	650	
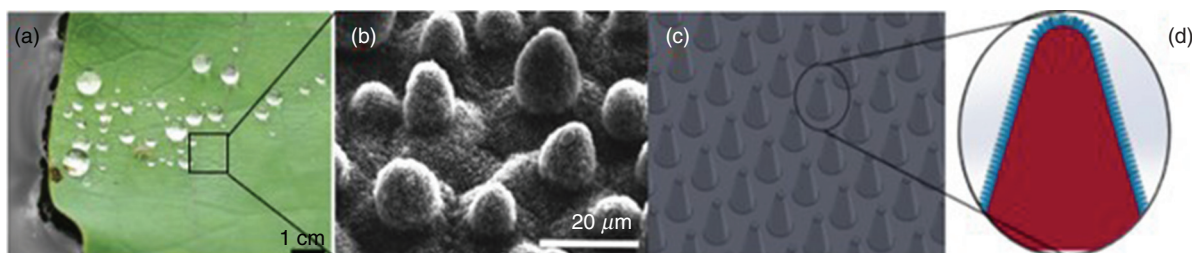
FIG. 22. (a) Natural lotus leaf. Reproduced with permission from G. S. Watson, D. W. Green, B. W. Cribb, C. L. Brown, C. R. Meritt, M. J. Tobin, J. Vongsvivut, M. Sun, A. P. Liang, and J. A. Watson, Applied Materials and Interfaces, **9**, 24381 (2017), Copyright 2017, ACS.[93] (b) Lotus leaf microstructure. Reproduced with permission from G. Carbone and L. Mangialardi, EPJ E, **16**, 67 (2005), Copyright 2005, Springer.[36] (c) Lotus leaf microstructure model (proposed CAD model corresponding to SEM image). (d) Lotus leaf micropapillae (red color) with nanobranches (blue color) (proposed CAD model corresponding to SEM image). Scale bar is 20 μm.
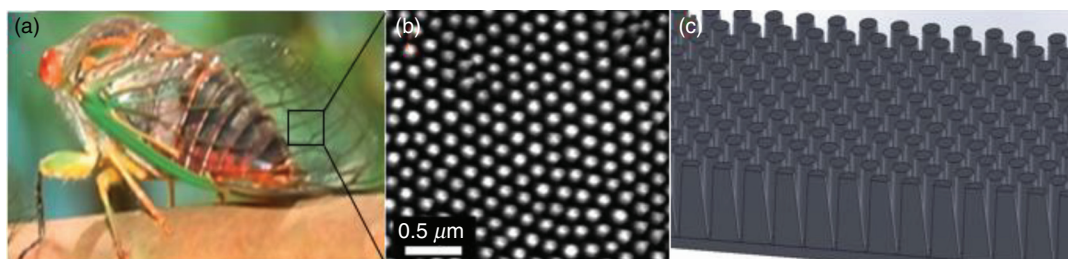
FIG. 23. (a) Cicada. Reproduced with permission from J. Hasan, R. J. Crawford, and E. P. Ivanova, Trends in BioTechnology, **31**, 295 (2013) Copyright 2013, Elsevier.[38] (b) Cicada wing under SEM. Reproduced with permission from G. S. Watson, J. A. Watson, S. Hu, C. L. Brown, B. W. Cribb, and S. Myhra, Int. J. of Nanomanuf. **5**, 112 (2010), Copyright 2010, InderScience.[96] (c) Cicada wing nanostructure model (proposed CAD model corresponding to SEM image).

enhanced when the features or dimensions are of the order of the bacterial size.

It can be observed that several works did not find any correlation between roughness and bacterial adhesion. However, it should be noted that the current approaches of characterizing surface roughness for the bactericidal effect typically rely on a single amplitude two-dimensional parameter, R_a,[110,112–116] which describes the arithmetical average value of the deviation of the trace above and below the center-line. The limitations of the use of the R_a parameter for surface characterization has been previously discussed.[117] Figure 28 shows an illustration of how completely different surface roughness can provide

the same R_a value. Thus, the analysis of roughness must involve other parameters and not just the R_a to understand how the surface roughness behaves against bacterial colonization. One way around this would be to characterize a surface in spatial frequencies.

Even though surface roughness is an influential parameter for bacterial adhesion, morphology is equally important.[18]

The morphology can vary depending on the manufacturing process, but some of the bactericidal examples can be grooves, pillars, pits, or nanotubes.

This highlights the importance of introducing 3D area surface characterization processes to provide a richer set of surface descriptors

FIG. 24. (a) Dragonfly insect. Reproduced with permission from C. D. Bandara, S. Singh, I. O. Afara, A. Wolff, T. Tesfamichael, K. Ostrikov, and A. Oloyede, ACS Appl. Mater. Interfaces **9**, 6746 (2017), Copyright 2017, American Chemical Society.[15] (b) SEM image of a dragonfly wing. Reproduced with permission from G. S. Watson, J. A. Watson, S. Hu, C. L. Brown, B. W. Cribb, and S. Myhra, Int. J. of Nanomanuf. **5**, 112 (2010), Copyright 2010, InderScience.[96] (c) Dragonfly wing model (Proposed CAD model corresponding to SEM image).
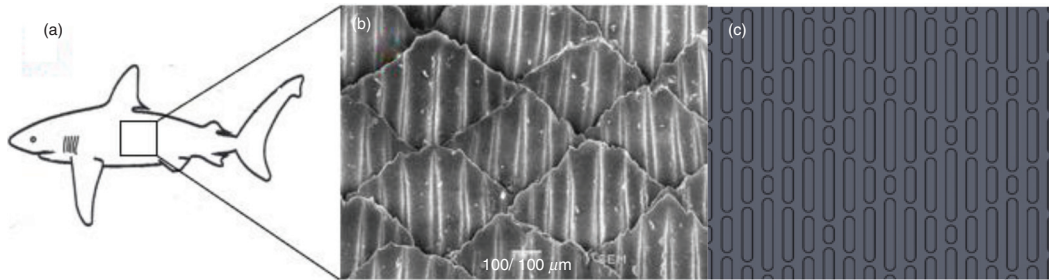
FIG. 25. (a) Shark. Reproduced with permission from D. W. Bechert, M. Bruse, and W. Hage, Exp. Fluids **28** (2000), Copyright 2000, Springer.[106] (b) SEM of the shark skin microstructure. Reproduced with permission from D. Y. Zhao, Z. P. Huang, M. J. Wang, T. Wang, and Y. Jin, J. Mat. Proc. Tech. **212**, 198 (2012), Copyright 2012, Elsevier.[54] (c) Model of the shark skin based on the Sharklet AF™ (proposed CAD model corresponding to SEM image).

(including height, spatial, hybrid, and functional properties) since it is anticipated this could provide a correlation with bactericidal effects, as previously suggested for other functionalities.[118]

Ercan et al.[119] manufactured Ti nanotubes with different diameters, varying from 20 to 80 nm. It was observed that the increase in the diameter decreases bacterial adhesion. Conversely, in the study carried out by Yu et al.,[120] where they manufactured Ti nanotubes from 30 to 120 nm, the increase in the diameters increased the bacterial adhesion.

Bandara et al.[15] tested *E. coli* bacteria and reported the interaction of the bacteria and the surface using a Transmission Electron Microscope (TEM) measuring system. A model was suggested to explain why bacteria rupture due to the nanopillar-based structures. Their proposed mechanism is shown in Fig. 29.

In another study carried out by Hochbaum et al.,[121] the spacing between pillars and the antibacterial effect was analyzed. Also, Lorenzetti et al.[122] studied the influence of the spacing of the grooves. Related to the dimensions of the features, Anselme et al.[123] made a concise review of the interaction between the nanostructuring of the surface and its effect on bacterial adhesion.

Wu et al.[124] fabricated pillar-like structures made by nano-replication technology in the polymeric material. Different models (with different sizes, heights, and spacings) were prepared and tested. They concluded that the density of the pillars had a critical impact on the bactericidal efficacy of the surface. Moreover, from this study it may be observed that the best model has a similarity with the dragon-fly wings. Apart from this study, a biophysical model of the bacterial stretching was developed where the stretching degree and the pillar density were evaluated.

Li et al.[125] created a thermodynamic model that predicted the nanopillar radius that ruptures the bacterial wall.

It should be noted that this model was only valid for Gram-negative bacteria due to their thinner bacterial wall.

Moreover, Cunha et al.[126] and Chan et al.[127] created structured surfaces by laser ablation on titanium samples. They both concluded

FIG. 26. (a) Gecko. (b) SEM image of the dorsal dorsum of the gecko animal. Reproduced with permission from G. S. Watson, D. W. Green, L. Schwarzkopf, X. Li, B. W. Cribb, S. Myhra, and J. A. Watson, Acta BioMaterialia **21**, 109 (2015), Copyright 2015, Elsevier.[12] (c) Scales at the micro-level creating the first level of the hierarchical structures (proposed CAD model corresponding to SEM image). (d) Cross-section view of the scales (red color) and the nanohairs (blue color) creating the second level of the hierarchical structure (proposed CAD model corresponding to SEM image).

FIG. 27. Illustration of the bactericidal effect and its root causes.
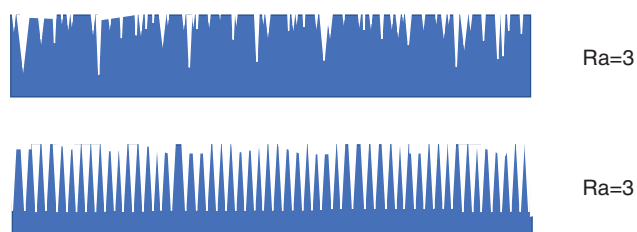
FIG. 28. Same surface R_a with differing morphologies.

that the enhancement of bacterial suppression was due to the similar dimensions between the bacterial diameter and the surface. This theory was also supported by other authors[18,117,128–130] due to the smaller contact area between the bacteria and the surface.

B. Wettability

The fundamental models of wettability of surfaces were discussed in Sec. II. Based on these known theories, several studies have attempted to clarify the effect of the wettability on bacterial adhesion.[14,117,128,131,132] Tang et al.[131] fabricated superhydrophobic surfaces on titanium samples, and they concluded that the superhydrophobic surfaces may inhibit S. aureus adhesion, with hydrophilic surfaces attracting S. aureus. Similar conclusions were drawn by Tripathy et al.,[10] Lee et al., or Fadeeva et al.[46]

Moreover, it has been reported that hydrophobic surfaces are able to reduce the adhesion of S. aureus.[133] Conversely, some studies concluded that bacterial repulsion was enhanced by hydrophilic surfaces.[126,131]

Thus, the extant literature does not clarify which type of surface repels S. aureus bacterial adhesion, superhydrophobic surfaces or hydrophilic surfaces.

C. Chemistry

The chemical composition of the surface can also alter bacterial adhesion. Campoccia et al.[134] proved that the chemical composition of the surface may alter bacterial adhesion. Researchers concluded that the crystalline structure of titanium oxide (the anatase phase) possesses more bactericidal activity than the amorphous phase.[127,135] The same conclusions were found by Del Curto et al.[136] and Giordano et al.[137] Chu and Williams[138] investigated the effect of the chemical composition of S. aureus and E. coli for response to different materials. Ivanova et al.[97] fabricated black silicon samples, inspired by dragonfly wings, using ion-beam etching and compared the bacterial adhesion to natural dragonfly wings. They concluded that the number of attached bacteria to the dragonfly-like textured black silicon was similar to those attached to the real dragonfly wing. This suggests that chemical composition has a minor effect compared to the surface topography. However, the effect that the removal of wax can play is known, as was discussed in Sec. II B 1, and this counteracts this conclusion.
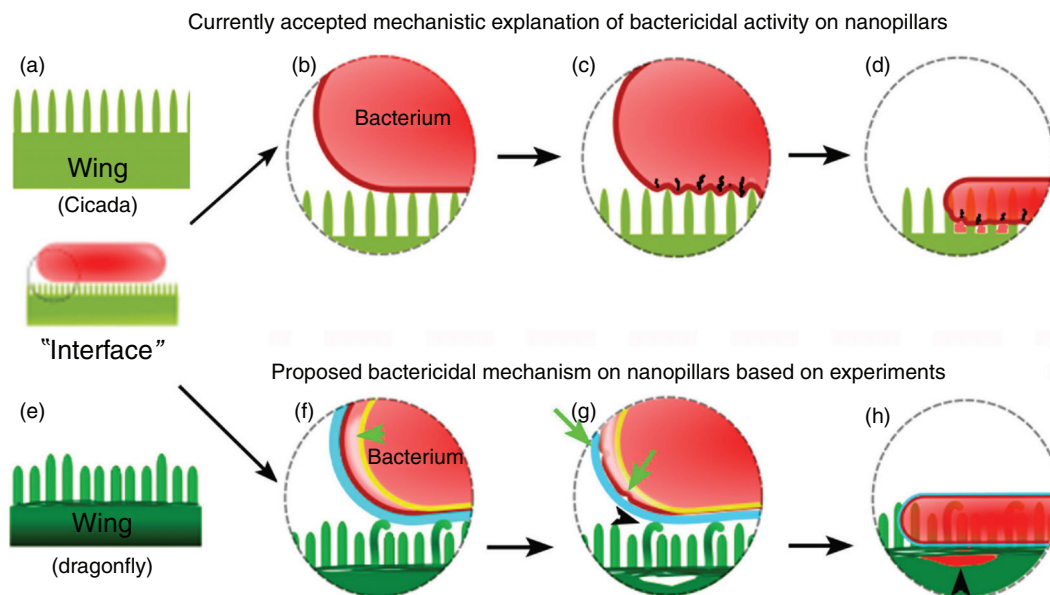
FIG. 29. Representation of the bactericidal mechanisms of the nanopillars. (a–d) Currently accepted mechanism between the interaction of bacteria-nanopillars. (e–h) Proposed mechanism. (a) Cicada wing nanostructure with tall pillar at the same height. (b) Bacterium approaching the nanostructure. (c) Bacterial membrane rupturing between the pillar-like structures due to stretching. (d) The bacteria get ruptured and the cytoplasm starts leaking, leading to bacterial death. (e) Dragonfly wing illustration with variable lengths of pillars. (f) The approaching bacterium bends the taller pillars, but it does not puncture the membrane. (g) After adhesive forces are applied to the bacterial surface, the two membranes (EPS in the blue and outer membrane in red)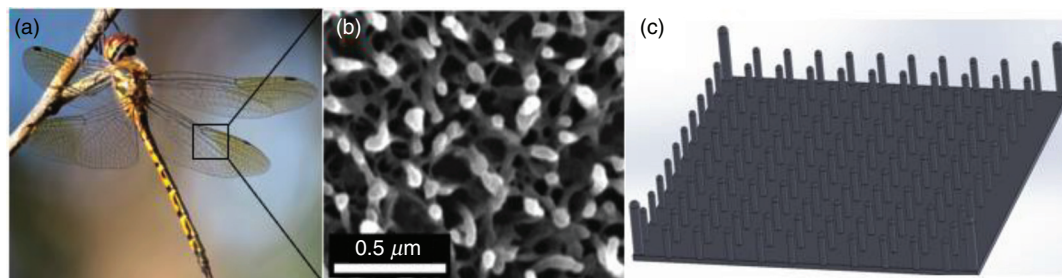 start separating. (h) Finally, the cytosol of the bacterium leaks, leading to cell death. Reproduced with permission from C. D. Bandara, S. Singh, I. O. Afara, A. Wolff, T. Tesfamichael, K. Ostrikov, and A. Oloyede, ACS Applied Materials and Interfaces **9**, 6746 (2017), Copyright 2017, American Chemical Society.[15]

1. Bactericidal activity of silver and copper

Over the last few years, special attention has been focused on introducing metallic nanoparticles such as Ag, Cu, Zn, or Au onto metallic or polymeric materials due to their high bactericidal activity.[139]

Silver is one of the most well-known natural bactericidal agents due to its high toxicity to most of the micro-organisms.[140]

It is believed that the bactericidal effect of silver relies on the interaction between silver ions and thiol groups of vital enzymes that passivates them. Several studies have been made on the interaction and use of Ag^+ ions to repel or kill bacterial strains.[141–143] These studies concluded that silver nanoparticles can repel the bacteria attachment by the rupture of their membranes.

Moreover, copper nanoparticles are also well-known for their bactericidal activity, employed for sterilizing liquids, textiles, or human tissues for over a few decades.[144] The current challenge relies on the synthesis of Cu nanoparticles because they undergo rapid oxidation into Cu^{2+} ions in air and in aqueous media.[145] Table V presents a comprehensive summary of the various types of particle used, doses employed and bactericidal response, as well as the manufacturing process employed to date in this regard.

2. Bactericidal activity of metal oxide nanoparticles

Despite silver being one of the most well-known bactericidal materials, many other nanoparticles are also known to cause bactericidal activity. Over the last few years, several metal oxide nanoparticles such as aluminum oxide (Al_2O_3), calcium oxide (CaO), magnesium oxide (MgO), or copper oxide (CuO) have prompted scientists to explore their antibacterial efficacy.[151] Moreover, the mechanism that explains the interaction between nanoparticles and bacteria is also reported by Slavin et al.[152] While they advocated the use of nanoparticles to rupture bacteria, they also highlighted that the antibacterial nanoparticles in high concentrations can be toxic and unhealthy.

Dizaj et al.[153] mentioned that the morphology of the nanoparticle has a big impact on the bactericidal effect: the surface/volume ratio of the nanoparticle. It was deduced that a smaller nanoparticle exhibits higher bactericidal effect.

Based on the reviewed literature[151–154] the main mechanisms of the bacterial metals, their characteristics and potential applications have been gathered in Table VI. Also, the antimicrobial effects of most used metal oxide nanoparticles are gathered in Table VII.

3. Bactericidal surface treatments obtained by silver ion implantation

Ion implantation, unlike a surface coating, allows an atomic species (in an ionized form) to penetrate onto the surface (sub-surface), which offsets the risk of delamination that is one problem with the coatings reported in the literature. Similar to other surface manufacturing processes, ion implantation improves the corrosion resistance, wear resistance, hardness, bioactivity, and antibacterial effect of biomaterials compared to their pristine forms. Since it is a surface modification technique, the favorable bulk properties of the substrates are preserved. In addition, one of the most valuable advantages of this low-temperature surface treatment technique is that it can strictly control the concentration and depth distribution of implanted ions by adjusting the processing parameters.

Among different ion implantation techniques, Plasma-Immersion Ion Implantation (PIII) is a suitable, versatile, and promising method for the surface modification of complex-shape materials without the line-of-sight limitations of conventional ion implantation techniques. Generally, a PIII system comprises a vacuum chamber with a workpiece stage, a plasma source, and a high-voltage pulse modulator. During PIII processing, samples are immersed in a high-density plasma and biased to a high negative pulsed potential relative to the vacuum chamber wall, which repels electrons away from the samples, while driving the positive ions of the plasma toward them, creating a plasma sheath around the samples.

Therefore, ions become implanted into the sub-surface, creating a thin sublayer in the range of a few tens of nanometers. In addition,

TABLE V. Bactericidal efficacy of different nanoparticles.

Nanoparticle	Dosses	Bacterial response	Manufacturing process	References
3 sizes of Ag	0.01 M	*S. mutans* reduction. Bactericidal response depends on the size.	Gallic acid in an aqueous chemical reduction method	146
Ag	4.26% using EDS	Remarkable antibacterial effect against *S. aureus* and *E. coli*	Silanization method	147
Ti nanotubes + Ag	0.5 M, 1 M, 1.5 and 2 M	Significant reduction of the osteoblast cells	Immersion in a silver nitrate solution	148
Ag+ + hydroxyapatite	296 mg/ml	More than 99% of *S. aureus* and *E. coli* were killed after 24 h	Dipping	149
Ag	25–100 mg/l	Concluded a 3-step process of P. Aeruginosa bacterial wall rupturing	-	141
Ag and ZnO	10 mM	Small reduction of *B. subtilis* bacteria reproduction	-	150

TABLE VI. Antibacterial mechanism for antibacterial metals, their characteristics, and potential applications.

Antibacterial mechanism	Corresponding antibacterial material	Characteristics	Prospective applications
Slow release metal ion sterilization	Copper, silver, metal ion phosphate antibacterial materials, etc.	High chemical activity provides long term and efficient slow release antibacterial material	Widely used in medical applications, stainless steel, water treatment. Prevent bask in liquid coatings and fabrics. But these materials tarnish easily and are expansive, which limits their applications
Slow release metal ion sterilization and photocatalytic sterilization	Hydroxyapatite, Ag-carrying phosphate antibacterial materials, etc	Phosphoric acid double salt has a strong adsorption function, large specific surface area, nontoxic, stable chemical properties; good combination of efficiency and lasting slow-release performance	
Slow release metal ion sterilization, photo-catalytic sterilization and reactive oxygen species antibacterial mechanism	ZnO materials, TiO2 materials	Stable chemical properties, under UV irradiation show broad spectrum antimicrobial properties, good pH stability, nontoxic, abundant raw material sources, low cost	Used in fiber, plastic, ceramic, coating, biomedical, and other fields

TABLE VII. Antimicrobial activity of metal oxide nanoparticles.

Metal oxide NPs	Test organism	Antimicrobial action
Aluminum oxide (Al_2O_3) NPs	*Escherichia col*	Growth inhibition of *Escherichia coli*
Antimony trioxide (Sb_2O_3) NPs	*Escherichia coli*, *Bacillus subtilis* and *Staphylococcus aureus*	Toxic to all the three microbes
Bismuth oxide (Bi_2O_3) NPs	*Pseudomonas aeruginosa*, *Acinetobacter baumannii* and *Escherichia coli*	No effect against all tested microbes
Calcium oxide (CaO) NPs	*Lactobacillus plantarum*	Higher bactericidal activity
Cerium oxide (CeO) NPs	*Escherichia coli*, *Shewanella oneidensis* and *Bacillus subtilis*	No effect on *Shewanella oneidensis*
Cobalt oxide (Co_3O_4) NPs	*Staphylococcus aureus* and *Escherichia coli*	Showed antimicrobial activity on tested bacteria
Copper oxide (CuO) NPs	MRSA, *Staphylococcus epidermis*, *Pseudomonas aeruginosa*, *Proteus* sp. *Staphylococcus aureus*, *Bacillus subtilis*, *Escherichia coli*; fish pathogens: *Aeromonas hydrophila*, *Pseudomonas fluorescens*, *Flavobacterium* sp. and *Branchiophilum* sp	Active against all the tested microbes
Magnetite (Fe_3O_4) NPs	*Escherichia coli*	Concentration-dependent bacteriostatic action
Iron oxide (FeO) NPs	*Staphylococcus aureus*, *Shigella flexneri*, *Escherichia coli*, *Bacillus licheniformis*, *Bacillus subtilis*, *Brevibacillus brevis*, *Vibrio cholerae*, *Pseudomonas aeruginosa*, *Staphylococcus aureus* and *Staphylococcus epidermis*	Moderate antibacterial activity against 6 Gram-positive and 2 Gram-negative bacteria
Magnesium oxide (MgO) nanowires	*Escherichia coli* and *Bacillus* spp.	Lower bacteriostatic activity

TABLE VII. (*Continued.*)

Metal oxide NPs	Test organism	Antimicrobial action
Titanium dioxide (TiO$_2$) NPs	MRSA	Exhibited antimicrobial effect on tested isolates
Zinc oxide (ZnO) NPs	MSSA, MRSA, and MRSE, *Streptococcus agalactiae*, *Staphylococcus aureus*, *Escherichia coli*, *Bacillus subtilis*, *Salmonella paratyphi*, *Staphylococcus aureus*, *Pseudomonas aeruginosa*, *Mycobacterium smegmatis*, *Mycobacterium bovis*, *Klebsiella pneumoniae*, *Enterobacter aerogenes*, *Candida albicans*, *Malassezia pachydermatis*, *Bacillus megaterium*, *Bacillus pumilus* and *Bacillus cereus*	Active on tested microbes
Zinc/iron oxide composite NPs	*Escherichia coli* and *Staphylococcus aureus*	Exhibited greater antibacterial activity with higher Zn/Fe weight ratio
ZnO-loaded PA6 nanocomposite	*Staphylococcus aureus* and *Klebsiella pneumoniae*	Dose-dependent antibacterial action
Nanosilver-decorated TiO$_2$ nanofibres	*Staphylococcus aureus* and *Escherichia coli*	Increased antimicrobial effect
Hybrid CH-α-Fe$_2$O$_3$ nanocomposite	*Staphylococcus aureus* and *Escherichia coli*	Improved antibacterial activity
Zinc-doped CuO nanocomposite	*Escherichia coli*, *Staphylococcus aureus* and MRSA	Remarkable biocidal activity
PEI-capped ZnO NPs	*Escherichia coli*	Exhibited better antibacterial activity
Chitosan-based ZnO NPs	*Candida albicans*, *Micrococcus luteus*, and *Staphylococcus aureus*	Showed biofilm inhibition against *Micrococcus luteus* and *Staphylococcus aureus*
Carvone functionalized iron oxide	*Staphylococcus aureus* and *Escherichia coli*	Inhibited colonization and biofilm formation
Silver-decorated titanium dioxide (TiO$_2$:Ag) NPs	MRSA and *Candida* sp.	Conferred antimicrobial effect on tested microbes
Graphene oxide modified ZnO NPs	*Escherichia coli*, *Bacillus subtilis*, *Salmonella typhimurium*, and *Escherichia faecalis*	Excellent antibacterial activity

NPs: nanoparticles; MRSA: methicillin-resistant *Staphylococcus aureus*; **MRSE: methicillin-resistant** *Staphylococcus epidermidis*; **MSSA: methicillin-sensitive** *Staphylococcus aureus*; **PEI: polyethyleneimine.**

consecutive etching, ion implantation, and deposition processes are possible by varying the processing parameters.

PIII technology offers unique advantages for treating various biomaterial surfaces. Previous shortcomings of poor coating adhesion (easy delamination) or roughness modification have been overcome by using PIII. Furthermore, PIII can be combined with different plasma ion sources: cathodic arc, metal vapor vacuum arc (MEVVA), electron cyclotron resonance (ECR), Kaufman, among others.

One of the promising applications of this technique is the possibility of creating antibacterial surfaces by the implantation of biocidal elements such as Ag, Cu, or Zn, or its combination with bioactive elements such as Ca and Mg.

Table VIII summarizes the main processing parameters (ion type, substrate, ion source, bias/acceleration voltage, and ion dose) and the bactericidal effect results obtained by silver ion implantation (and its combination with other elements) conducted by different research groups.

It can be observed that most of these works have demonstrated a bactericidal efficacy against *E. coli* and *S. aureus*. However, it has also been shown that silver ion implantation treatments are effective against a number of pathogens found in infectious processes such as peri-implantitis: *P. gingivalis*, *A. actinomycetemcomintas*, *P. aeruginosa*, *C. albicans*, *S. mutans*, *A. actinomycetum*, *F. nucleatum*, *B. forsythus*, among others.[155–159]

It should be noted here that some of these studies report that the silver ions implanted in the surface agglomerate in the form of nanoparticles. Despite the potential toxicity of nanoparticles, an *in vivo* study carried out by H. Qin *et al.*[155] on Labrador dogs demonstrated that the treatment is not only biocompatible but also favors osseointegration, arguing that the plasma immersion ion implantation technique reduces the mobility of the nanoparticles and promotes, in turn, cytocompatibility.

Similarly, an *in vivo* study on Sprague Dawley rats conducted by Mei *et al.*[156] established the optimal bias voltage for obtaining a bactericidal effect without causing any inflammatory phenomena due to the possible toxicity of silver.

TABLE VIII. State of the art of bactericidal treatments based on silver ion implantation.

Ion	Substrate	Plasma ion source	Bias/Acceleration voltage (kV)	Dose ions/cm^2	Bacteria tested In vivo studies	Reference
Ag	Ti	ECR	2	$1.5 \cdot 10^{16}$	S. aureus	162
Ag	Ti	Cathodic arc	30	-	E. coli, S. aureus	163
Ag	Ti	Cathodic arc	20	-	In vivo positive response	161
Ag	Ti	MEVVA	40	10^{16}	S. aureus	164
Ag	Ti	Cathodic arc	15	-	F. nucleatum, S. aureus	159
Ag	TiO$_2$-Ti	MEVVA	70	$10^{17} - 2 \cdot 10^{18}$	S. aureus	165
Ag	316LVM	Cathodic arc	30	-	E. coli, P. aeruginosa, S. aureus, S. epidermis	155
Ag	TiO$_2$	MEVVA	40	$(0,5-10) \cdot 10^{16}$	E. coli	166
Ag	Ti	Cathodic arc	30	-	In vivo positive response Osseoconductive treatment	167
Ag	TiO$_2$-Ti	Cathodic arc	0,5-1	-	P. gingivalis, A. actinomycetemcomitans. In vivo positive response	156
Ag	CrN-316L	Kaufman ion source	100	$5 \cdot 10^{16}-10^{17}$	E. coli, S. aureus	168
Ag	TiO$_2$-Ti	MEVVA	65	$(1-20) \cdot 10^{17}$	S. aureus	169
Ag	AISI 420	MEVVA	50	10^{17}	E. coli	170
Ag	Ti	Cathodic arc	15	-	S. mutans. P. gingivalis, C. albicans	157
Ag	Ti	——	15	10^{16}	A. actinomycetum, F. nucleatum, C. rectus, P. micros, B. forsythus	158
Ag	Ti	Cathodic arc	30	-	E. coli, S. aureus	171
Ag	317L, TiN-317L	MEVVA	70	$5 \cdot 10^{16} - 5 \cdot 10^{18}$	S. aureus	172
Ag	Pyrolytic carbon	MEVVA	70	$5 \cdot 10^{14}- 5 \cdot 10^{18}$	E. coli, S. aureus	173
Ag/Zn, Ag+Zn	Ti	Cathodic arc	30	-	E. coli, S. aureus. In vivo positive response	174
Ag, Ag+Mg	Ti	Cathodic arc	30-40	-	E. coli	175
Ag/Ca, Ag+Ca	Ti alloy	MEVVA	50	10^{17}	E. coli, S. aureus	176
Ag/Zn, Ag+Zn	Ti	Cathodic arc	30	-	E. coli, S. aureus. In vivo positive response	160
Ag+Cu	AISI 420	MEVVA	50	$2 \cdot 10^{17}$	S. aureus, A. niger	177
Ag/Cu	Ti6Al4V	CHORDIS	2-20	$10^{15}-10^{17}$	E. coli, S. aureus	178
Ag/Cu	Polyethylene	Cathodic arc	5	-	E. coli	179
Ag/Cu	317L, Ti, TiAlNb	MEVVA	80	10^{17}	S. aureus	180

Another *in vivo* study on Sprague Dawley rats demonstrated the synergistic bactericidal and osteogenic effect provided by silver and zinc nanoparticles obtained by the simultaneous ion implantation of both elements using cathodic arc sources.[160]

More recently, Cao *et al.* demonstrated the osteogenic effect of bone marrow stem cells induced by silver ion implantation on implants inserted in rats.[161]

4. Bactericidal carbon-based coatings doped with silver

In the last two decades, amorphous diamond-like carbon (DLC) coatings have received great interest due to their exceptional properties, such as high hardness, low friction, chemical inertness, corrosion protection, biocompatibility, optical transparency in the IR spectral range, and tunable electrical resistivity.[181,182] Nowadays, DLC coatings have been industrially implemented in many engineering applications where excellent tribological properties are required. Additionally, the outstanding biocompatibility of these coatings offers a wide range of potential biomedical applications for the improvement of the mechanical, chemical, and biological response of prostheses and implants.[183] Specifically, the possibility of doping DLC coatings with bactericidal elements such as silver has resulted in intensive research in this field.

The main bactericidal effect of silver is conducted through the release of Ag$^+$ ions via an oxidative reaction in an aqueous solution or a biological medium.[184]

The kinetics of this dissolution process relates to the duration of the antibacterial effect, can increase exponentially if silver is used as nanoparticles due to its higher surface to volume ratio. Furthermore, the stability and the long-term antibacterial effect of Ag-doped DLC depends on various factors, such as surface energy, mean roughness, micro- and nanostructure of the coating, as well as the concentration and distribution of silver across the thickness of the coating (dispersed or agglomerated in the form of nanoparticles).

Various methods have been reported of preparing Ag-DLC coatings with different silver concentrations specifically for biomedical applications, which include radio frequency (RF) or direct current (DC) reactive magnetron sputtering of the silver target in a hydrocarbon atmosphere,[185–193] DC magnetron sputtering of silver and graphite targets,[194–196] hybrid RF/magnetron sputtering plasma assisted chemical vapor deposition (RF/MS PACVD),[197,198] dip coating of a PVP polymer film with a colloidal dispersion of stabilized silver nanoparticles transformed to DLC by ion implantation,[199–201] polyethylene transformed to DLC by silver implantation,[202,203] thermionic vacuum arc,[204] silver nanoparticle solution combined with a DLC coating obtained by PACVD,[205] cathodic arc deposition,[206–210] and pulsed laser deposition.[211–215] Most of these works demonstrate good antibacterial efficacy of these coatings against *E. coli*, *S. aureus*, and *S. epidermidis* for silver concentrations higher than about 2 at. %. Also, Ag-doped DLC coatings offer an antibacterial activity over a wide spectrum of other bacterial species: *C. jejuni* and *L. monocytogenes*;[192] *A. israelii*, *S. sanguinis*, *F. nucleatum*, *C. rectus*, *E. corrodens*, *P. micra*, *P. intermedia*, *A. actinomycetemcomitans*, and *P. gingivalis*;[196] *S. warneri*;[212] and *P. aeruginosa*, *E. faecalis*, and *C. albicans*.[215] On the other hand, good hemocompatibility of DLC coatings with a silver concentration of 9.7%,[185] and between 70% and 90%[209] has been demonstrated. Furthermore, Chekan *et al.*[210] have shown that DLC coatings doped with a silver concentration of 3.5% to 6.5% possess an inhibiting effect on the growth of some tumor cells.

Despite good antibacterial efficacy shown by Ag-doped DLC coatings, the main concern related to its applicability in prostheses and implants lies in the adjustment of the optimal concentration of silver to obtain a significant antibacterial activity by suppressing cytotoxicity. In this sense, coatings with a silver concentration as low as 1.6% and 2.1% have shown significant levels of cytotoxicity.[191] Other studies point to silver concentration thresholds of 4.5%[201] or 5.4%,[197] above which the coating becomes cytotoxic. In this regard, excellent non-cytotoxic properties have been reported for DLC coatings with silver concentrations of 2.0%[198] and 3.1%.[193] On the contrary, non-cytotoxic coatings have been obtained for silver concentrations of 5.6%[206] and 6%.[196] More detailed studies demonstrate that the adequate concentration of silver, in terms of physical-chemical properties, for providing an efficient protection against microbial colonization and a non-cytotoxic behavior, ranges between 2% and 7%,[213] and more accurately 3.6%.[215]

The disparity of these results reveals that the antibacterial activity and cytotoxicity of these types of coating not only depends on the concentration of silver, but, as mentioned above, other factors determine the kinetics of the release of Ag^+ ions. However, given the published results, a conservative value of the concentration of silver that guarantees an antibacterial effect without causing cytotoxicity would be around 2%.

D. pH, ionic strength, and temperature

In most of the studies, a lot of importance has been attributed to the surface wetting, chemical composition, or morphology. However, since bacterial adhesion is governed not only by one surface property, a small change in the pH of the environment, ionic strength, or temperature around the implant may also alter bacterial adhesion. For example, the effect of the ionic strength was explored by Morisaki *et al.*[216] Also, Hamadi *et al.*[217] studied the effect of the pH on bacterial adhesion, and they concluded that less bacterial adhesion was observed on the extreme values (2 and 12), whereas at a pH of 5, most bacteria flourish. Garret *et al.*[218] presented a very comprehensive review illustrating the effect of the pH and temperature on the bacterial colonization.

IV. ULTRA-PRECISION MANUFACTURING OF BIOMIMETIC SURFACES

In this section, various nano- and micro-manufacturing methods applied to date for producing patterned biomimetic surfaces are reviewed to highlight and discuss the limitations and advantages of each technology.

According to Bruzzone *et al.*[219] and Jaggessar *et al.*,[45] various surface modifications can be divided into three streams as additive methods, subtractive methods, or re-structuring (patterning—theoretically involving no loss or addition of material onto the surface). Moreover, according to Mijatovic *et al.*[220] and Biswas *et al.*,[221] the additive method is referred to being a bottom-up method, and the subtractive method is referred to as a top-down method.

Figure 30 shows an overview of the classification of the different manufacturing techniques employed to modify the surfaces.

A. Additive processes

Additive methods rely on adding the material to the desired surface. Most of those methods are related to the deposition of coatings or implantations. Table IX summarizes various additive methods reviewed by Bruzzone *et al.*[219]

The chemical processes shown in Table IX involves printing the surface with inks that can inhibit or promote some chemical or

Additive methods	• Chemical routes • Physical routes
Subtractive methods	• Beam based routes • Mechanical routes • Chemical etching
Surface patterning methods	• Chemical routes • Mechanical routes • Re-structuring routes

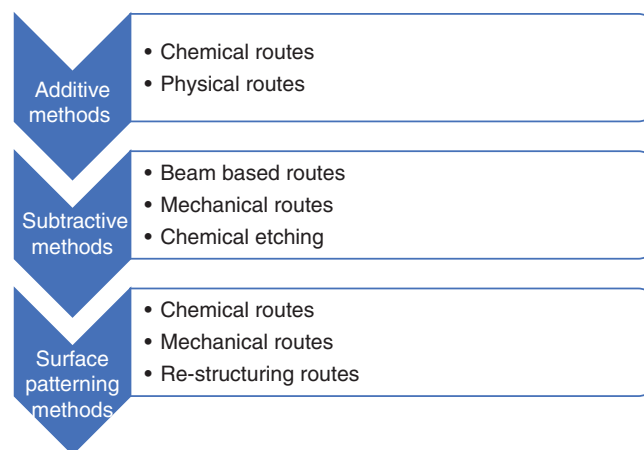**FIG. 30.** Overview of the manufacturing techniques classification.

TABLE IX. Classification of additive type surface modification techniques.

Additive processing		
Chemical processes	Chemical conversion coating	Patterned chromating
		Patterned phosphating
	Chemical deposition coatings	Chemical vapour deposition (CVD)
		Patterned autocatalytic plating
		Anodising
		Electro-deposition[a]
		Sol-gel
Physical deposition	Patterned precipitation coating	
	Inkjet	
	Patterned curing	
	Physical vapour deposition (PVD)	
	Painting	
	Deposition of micro- or nanoparticles[a]	
	Self-assembling in polycrystalline films[a]	
	Vacuum casting	

[a]Considered as an ultra-precision manufacturing technique.

electrochemical reactions, so some patterned coatings can be achieved.[219] These, for instance, include Roll-to-Roll (R2R) manufacturing routes, which have started to become an ultra-precision fabrication technology.[222] In the past, anodizing processes have been used[137,223–225] to inhibit bacterial colonization. Driven by an electrolysis approach, this process consists of chemical reactions between a cathode and an anode leading to thin film formation on the surface.[8] Also, chemical vapor deposition (CVD) has been employed[226–228] with different particles in order to avoid bacterial adhesion on different surfaces as well as physical vapor deposition.[229] CVD is a chemical reaction-based method that is used to fabricate advanced functional surfaces. Different types of CVD methods can be used such as plasma-enhanced CVD, catalyst assisted CVD, or initiated CVD. The major limitation of this method of harnessing advanced and complex surface functionalities lies in the difficulty in controlling the precision of the surface detail.[37] Park et al.[230] fabricated

a multifunctional surface based on nanotaper structures (based on pitcher plants), which gave them antifogging and superhydrophobic abilities.

The deposition of micro- or nanoparticles has also been used to reduce bacterial adhesion. Ion implantation is another technique used in this area.[9,231] The particles are implanted between 0.1 and 1 μm depth.[232] It has been reported that Ag, Cu, Zn-Ag, and Ca ions have been used for S. aureus suppression.[174,176,178,180,233,234] Table X summarizes the additive fabrication techniques used to create bactericidal surfaces.

B. Subtractive processes

These methods consist of creating small depressions or features by removing the material from the surface.[219] Table XI summarizes the common subtractive routes.

TABLE X. Additive manufacturing processes employed to suppress the bacterial adhesion.

Additive process	Materials employed	Bacterial response	Reference
Anodization	Grade 2 Ti and Ti6Al4V	Successful bactericidal activity of the anodized samples	137
Nanoimprint lithography	PMMA	50% decrease of E. coli bacteria compared to polished ones	235
Electrodeposition	Au nanoparticles	All structures Au nanoparticles exhibit great bactericidal activity against S. aureus	236
Physical vapour deposition	Titanium coated with copolymers	Decrease of the S. aureus bacteria.	237
Spraying deposition	Titanium anodized substrate coated with polylactide.	0.5% of PLA concentration showed the best inhibition rate to S. aureus.	238

TABLE X. (*Continued.*)

Additive process	Materials employed	Bacterial response	Reference
Lyophilization method	Titanium nanotubes loaded with gentamicin	Reduction of *S. aureus* and enhance osteoblast activity	239
Physical vapour deposition	Grade 2 Ti with silver coating	Reduce the bacterial adhesion of *S. epidermidis* and *K. pneumoniae*.	229
Chemical vapour deposition	Silicone elastomer	Decrease of *S. aureus* bacteria compared with uncoated sample	240
Ag and Cu Ion implantation	317L, Pure Ti, TiAlNb	Improved the antibacterial properties of the substrates	178,180

Laser ablation or photoablation rely on using high energy concentrations to ablate the material from a solid (or occasionally liquid) surface by irradiating it with a laser beam. One of the major advantages of this method is that this technique can very conveniently be adopted to process free form surfaces to create surface textures.[241,242] To date, several laser types have been developed such us, excimers, solid state lasers, copper vapor, CO_2, Ti:Sapphire, or diode.[243,244] Moreover, some effects of the laser have been reported such as wavelength, pulse width, or scan speed as well as the differences between femtosecond, nanosecond, and picosecond[244–250] pulses. Several studies used femtosecond lasers[46,126,251] and nanosecond lasers[252–256] on different materials to create structured bactericidal surfaces. Figures 31 and 32 show examples of laser structured surfaces reported in the literature.

Chen *et al.*[254] fabricated groove like structures with different spacing [Fig. 32(a)] on titanium samples to evaluate the cell response.

Unlike laser processing, acid etching relies on immersing the substrates in strong acids such as HCl, H_2SO_4, or HNO_3 to allow material removal from the surface gently.[9] Giner *et al.*[257] carried out a study, where titanium disks were cut and etched to study their cell response. It was observed that this method was able to alter the cell response and the contact angle of the surface. Moreover, Zinelis *et al.*[258] evaluated the surface properties and elemental alterations produced by EDM on some dental implants. Also, Geim *et al.*[259] fabricated gecko-inspired surfaces using oxygen plasma etching made of polyimide pillars capable of supporting large masses.

Latthe *et al.*[260] reported in their review paper different wettings of the superhydrophobic lotus leaf apart from some techniques used to artificially mimic this surface. Table XII summarizes various subtractive routes used in the past for the creation of bactericidal surfaces on different materials and their influence on bacterial activity.

TABLE XI. Classification of the removal of material surface modification techniques[45,219] by subtractive routes.

| Beam based methods	Laser methods		Laser texturing (LT)
			Masked excimer laser
			Laser honing
			Focused ion beam
			CNC focused laser
			Femtosecond laser
	Electrical discharge machining (EDM)		Electrical discharge texturing (EDT)
			Micro EDM
	Ion beam texturing		
Chemical etching	Masking methods		Chemical texturing
			Electrochemical texturing
	Non-masking methods		Self-assembling
			Maskless laser assisted etching
			Maskless electrochemical texturing
			Anisotropic etching
Mechanical	CNC ultrasonic machining		
	Mechanical honing		
	Precision Grinding		
	Free abrasive machining		
	Microcutting		
	Patterned erosion		
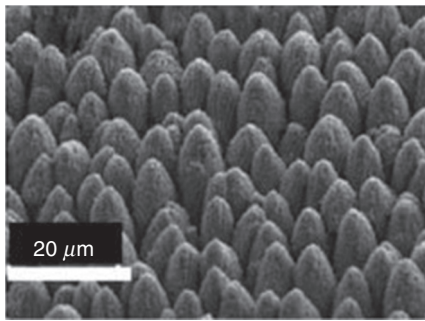
FIG. 31. Femtosecond laser processed cone type structure on titanium material. Reproduced with permission from B. K. Nayak, M. C. Gupta, and K. W. Kolasinski, Applied Physics A **90**, 399 (2008), Copyright 2008, Springer.[251]

C. Re-structuring or patterning

Re-structuring is based on changing the surface structure by plastic deformation and redistribution of material from one part to another. According to Bruzzone et al.,[219] this stream encompasses various processes, as shown in Table XIII.

During shot blasting, hard small particles impact the substrate at high velocity, causing roughening of the surface layer. In this technique, it is difficult to precisely control the texture due to the shape, velocity, and hardness of the particles, and the randomness in contact is also difficult to control. It should be noted that shot blasting creates random surfaces.[9] Soboyejo et al.[252] apart from using laser processing, used alumina blasting to modify the surface of a medical device. Bürgers et al.[262] carried out an experiment where samples were modified by blasting with subsequent acid etching and machining. An increase in bacterial adhesion was observed on blasted and subsequently acid-etched samples.

Surface wrinkling is an easy to control fabrication method, and one of its advantages is that the surfaces can be easily controlled up to micro/nanoscale.[37] Also, surface wrinkling is characterized by its good tunability and reversibility compared to other patterned techniques.[266]

Jiang et al.,[267] using the lithography surface modification technique, created micro-cylinders made of silicon inspired by the lotus leaf. They performed a bacterial test (E. coli) to compare a fresh and a silicon lotus leaf. They observed that in the initial 3h of incubation, no bacteria were attached to the surfaces, resulting in the advanced hydrophobic property of the surfaces. After 24h of incubation, some bacteria remained attached to the surface, suggesting the air trapped between the microstructure played an essential role in impeding bacterial adhesion.

Also, vibrorolling uses gentle plastic deformation of metals. Usually, a hard metal or a diamond is used to advance into the surface creating uniform texture with regular-shaped asperities.

D. Surface property impact of manufacturing techniques

A classification of the most used manufacturing methods for creating bactericidal surfaces and their impact on the surface properties has been made in Table XIV. The final discussion on the metrology aspects of the surfaces is made in Sec. V.

TABLE XII. Subtractive manufacturing processes employed to create bactericidal surfaces.

Subtractive process	Materials employed	Bacterial response	Reference
Femtosecond laser	Ti6Al4V	Similar bactericidal (S. aureus) response between nanopillars and LIPSS.	126
Femtosecond laser	Ti6Al4V	Colonisation of S. aureus on all the laser treated surfaces but rejection of P. aeruginosa and S. mutans on nanopillar like structure.	253
Nanosecond laser	Ti6Al4V	Biofilm formation of E. coli and S. aureus on non-treated surface but bacterial attachment was not avoided.	261
CW laser	Ti6Al4V, CoCrMo and CpTi (Grade 2)	The most bactericidal surface was observed on the CpTi against S. aureus which exhibits the lowest CA (31.9°)	127
Machining vs Sand blasting + acid etching	Pure Ti	Machined samples showed better bactericidal activity S. sanguinis than acid treated ones.	262
Polishing vs grit blasting vs	Ti6Al4V	Polished surface showed lowest	108

TABLE XII. (*Continued.*)

Subtractive process	Materials employed	Bacterial response	Reference
plasma sprayed vs satin		*S. epidermidis* adhesion continued by plasma spraying, grit-blasting and sating.	
Chemical oxidation	Grade 2 Ti	Avoid bacterial adhesion of *S. aureus* and *E. coli* compared to smooth one.	263
Plasma glow discharge	PVC	Significant decrease of the *P. aeruginosa* bacteria.	264
Plasma treatment	Polymeric suture materials	Reduction of *E. coli* bacteria depends on the available contact area.	265

TABLE XIII. Classification of the re-structuring surface modification techniques.[45,219]

Re-structuring		
Mechanical	Shot blasting	
	Embossing	Vibrorolling
		Patterned embossing tools
		Lithography
		Wrinkling
		Photolithography
Chemical	Molecular migration	
	UV contraction	

V. METROLOGY OF PRECISION PATTERNED BIOMIMETIC SURFACES

This section is dedicated to the measurement or metrology of precision fabricated surfaces. In this section, the most recent and most common surface characterization techniques are briefly reviewed, comparing their functional features and resolutions by identifying advantages and disadvantages that will benefit and facilitate characterization of bioinspired fabricated surfaces; further information can be found from the relevant sources in the literature.[270,271]

Although several techniques are available for surface metrology measurements, most of them use electrons, photons (light), x-ray, ions, or other types of particles or waves, to interact with the surface undergoing testing. In some cases, surface information is derived from tracking the changes induced by the exciting beam. In many others, the information comes from analyzing the return signal provided by the samples.

Metrology measurements may require physical contact between probe tips of the measurement device and sample under test, often leading to destruction of the sample's surface; this is called contact metrology. Other methods, mainly optical based, which do not require any physical contact with the samples, are referred to as contactless metrology.

Figure 33 shows typical specification (resolution) of the most popular and most advanced methods for modified surface metrology measurements involving contact and non-contact modes of measurement in the form of a Stedman diagram.[273] For each characterization method, there exists many variations (sub-methods) of similar analytical techniques. It is important to emphasize that nowadays the technology is improving rapidly, therefore this illustration can only be used as a reference and not to infer absolute values.
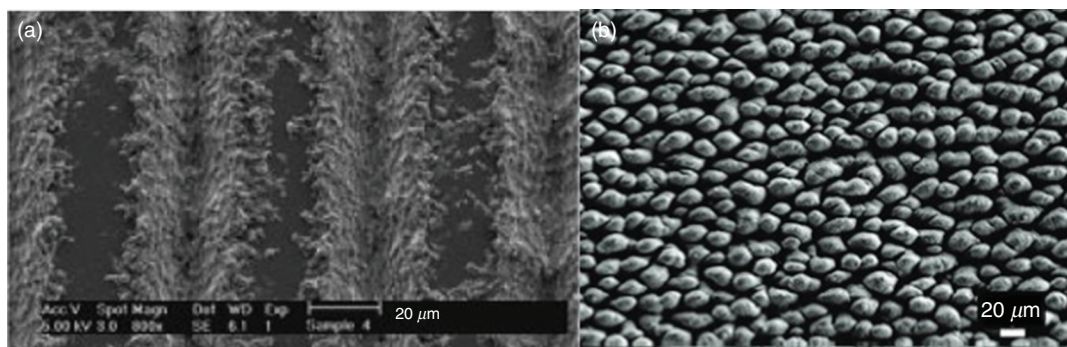
FIG. 32. (a) Ti6Al4V sample with 50 μm separation tracks. Reproduced with permission from J. Chen, S. Mwenifumbo, C. Langhammer, J.-P. McGovern, M. Li, A. Beye, and W. O. Soboyejo, J. Biomed. Mat. Research Part B: Appl. Biomater. **82B**, 360 (2007), Copyright 2007, Wiley,[254] and (b) laser processed titanium sample inspired by a lotus leaf. Reproduced with permission from E. Fadeeva, V. K. Truong, M. Stiesch, B. N. Chichkov, R. J. Crawford, J. Wang, and E. P. Ivanova, Langmuir **27**, 3012 (2011), Copyright 2011, ACS.[46]

TABLE XIV. Impact of the surface properties of different manufacturing techniques.

| | Surface property impact | | | | |
Technique	Chemistry	Wettability	Topography	Other	Reference
Femtosecond laser	Medium	Strong	Strong (nanoscale, microscale)	No surface damage	46,126,253,268
Nanosecond laser	Medium	Strong	Medium (microscale)	Surface damage	261,269
Ion Implantation	Strong	Weak	Weak	-	179,180
Anodization	Weak	Weak	Weak	-	137
Chemical oxidation	Strong	Strong	Strong (nanoscale)	-	263
PVD	Strong	-	Medium (microscale)	-	229,237
CVD	Strong	Medium	Medium (microscale)	-	240

A. Contactless metrology

Contactless metrology using optical methods coupled with advanced CCD/CMOS cameras can provide fast measurements on large areas without damaging the surface. However, the resolution of these devices is limited by the wavelength of the electromagnetic radiation used (Rayleigh criterion) and optical aberration, which is the most difficult challenge to overcome in order to reach low resolutions.

Optical microscopes consist of a light source that emits electromagnetic radiation passing through an optical system to project the sample under investigation. The optical systems are designed using different techniques, such as **confocal microscopy**, where resolution

FIG. 33. Stedman diagram: Typical resolutions of some common metrology used to assess surface modified fabrication methods. Reproduced with permission from H. Villarraga-Gómez, L. Körner, R. Leach, and S. T. Smith, J. Prec. Eng. **64**, 228 (2020), Copyright 2020, Elsevier.[272]

and contrast are improved by filtering the scattered diffraction, removing the out-of-focus light. Monochromatic confocal microscopes use lasers whereas confocal chromatic systems use white light as the source. Surface information of the sample is extracted by reading and analyzing the optical feedback signal from the sample, which could be fluorescence or a spectrum of reflected light. The most advanced confocal microscope can reach 0.1 μm depth resolution over a 1 mm measurement range (Fig. 33). The optical microscope remains one of the most useful and cost-effective tools for surface metrology in terms of measurement speed, effectiveness, and versatility of use.

Optical profiler is a contactless, vertical scanning, white light or laser interferometer that can be used to characterize and quantify surface roughness, height distribution, or other topographical features. It can use 2D or 3D operations with depth resolution ranging from ~1 to 5000 μm, and ~10 μm/s scanning speed.

Scanning electron microscopes (SEM) operate with a similar principle to optical microscopes, but instead of using an optical beam (laser or white light), the SEM focuses an electron beam on the sample surface and collects the feedback signal to map the sample surface topography. The feedback signal is normally the number of secondary electrons emitted by the excited atoms of the sample surface. SEM can provide lateral resolution as small as 1 nm. However, as the electron beam must be raster scanned, there is a limit to the sample size, typically < 10 cm. In addition, an electron beam must operate under vacuum so the sample must be compatible with it. From topographical characterization, the major disadvantage is the inability of the conventional SEM to measure in the third dimension, or depth of topographical features. Even though in the past two decades some stereology techniques have been developed to obtain quantitative 3D information,[274] it is usually used qualitatively and as a lateral quantity only, rather than as a primary surface measurement instrument.

Dynamic force microscopes, such as Electrostatic Force Microscopes (EFM), are non-contact but not optical based methods. In EFM, a cantilever sensor tip is held at ~1 to 100 nm from the sample surface. This distance is large enough to avoid collision between the tip and the sample's surface. Applying a biased voltage (AC or DC) between the conductive cantilever and the sample can create an electrostatic force that can be probed and mapped while scanning the sensor tip over the surface of the sample. EFM is a promising method for sub-micrometric surface measurements, but it works only with electrically conducting samples, making it appropriate for characterizing medical implants.
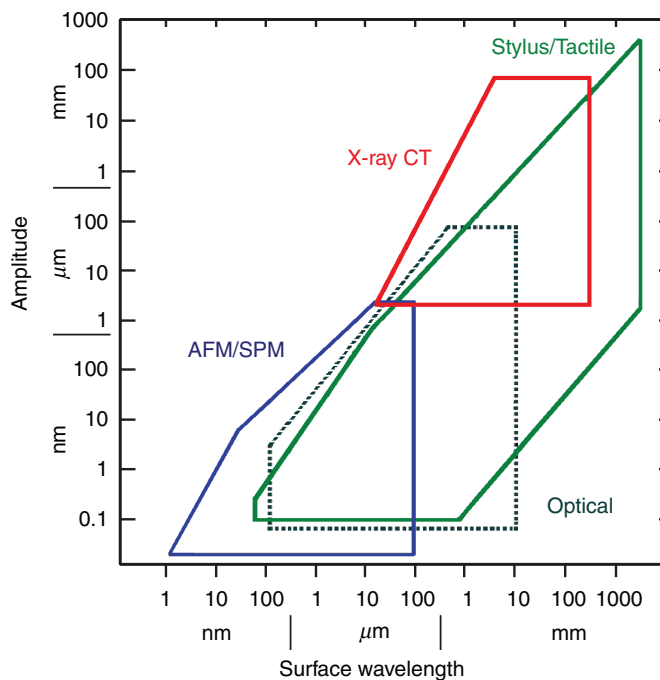
B. Contact metrology

Contact metrology may have better resolution than contactless methods, but this approach often leads to small scale plastic deformation (of a destructive nature) on the sample surface intended to be measured.

For the characterization of surface topography at the nanometer level, an Atomic Force Microscope (AFM) is a powerful tool. It consists of a probe tip of a nanometer size located at the free end of a cantilever. When the tip approaches the sample surface, it reaches a critical distance as small as the atomic level (a few angstroms), resulting in the cantilever experiencing a bending force arising from van der Waals forces. This bending level can be measured by a position-sensitive detector. Unlike EFM, AFM does not measure the tunneling current between the probe tip and the surface, instead it measures the direct interaction at the atomic level between the two and, hence, is a contact measurement method. The lateral resolutions of an AFM depend on the size of the probe tip, typically < 1 nm, whereas the depth resolution depends on the sensitivity of the position sensitive detection, which could be as small as 0.1 nm.

A stylus profiler is typically a one-and-a-half-dimension coordinate measurement machine that operates based on the mechanical principle. It is very useful for surface roughness and topography measurements because its measurement range is very large. It consists of a stylus with a micrometer or sub-micrometer probe tip that moves up and down while scanning around the sample surface. The sample surface topography information is then reconstructed based on the up and down data measured. This method gives a quick result on almost any type of material.

VI. FUTURE RESEARCH DIRECTIONS AND CONCLUSIONS

The idea of creating antibacterial materials by modifying the surfaces needs to be exploited in more detail. To create new generation advanced medical materials, deep research is required. This review hinted at some possible future research endeavors from which future researchers could benefit.

First, it was observed that the effect of chemistry, in Sec. III C, repulsing bacterial adhesion has a minor effect. Nevertheless, it has been reported that removing wax from the lotus leaf, in Sec. II B 1, from the surface has a significant impact on the surface hydrophobicity. Thus, more studies are required to clarify the effect of surface chemistry on bacterial adhesion. From the literature on this topic, we also noticed some contradictory results, for example, Yang and Deng[133] reported that hydrophobic surfaces prevent bacterial adhesion whereas Cunha et al.[126] reported that hydrophilic surfaces avoid bacterial adhesion.

No direct evidence was found in support of the argument that the wetting angle has a direct correlation to bacterial attachment. Certainly, a wetting contact angle speaks to the surface energy, but this review asks a key question, can this alone describe the nature of bacterial attachment? This review highlighted that in some cases a change in the contact wetting angle on the surface may not necessarily confirm that the surface is bactericidal, and biological laboratory tests would be required to unambiguously prove that the modified surface is bactericidal.

What was also learned from this review was that most of the cartoon models explaining the bacterial killing from the spikes on the surfaces assume the bacteria to be isolated from the environment, whereas in reality a bacterial testing process is carried out in a broth to provide nutrients to the bacteria, and while some bacteria are killed by the bactericidal surfaces, the other bacteria in the broth keep proliferating. Thus, fabricating a bactericidal surface capable of killing all bacteria in the broth at once is unlikely, and current models do not capture this aspect. This knowledge gap mandates the necessity of undertaking laboratory-scale, pre-clinical and post-clinical examination of the bactericidal surfaces. The only thing that may be speculated is that the surfaces should aim to suppress the probability of bacterial infection. Complete eradication of bacterial growth by making nature-inspired fabricated surfaces is merely a hypothesis.

The published literature available on bactericidal surfaces does discuss the influence of surface roughness on bacterial attachment, i.e., the parameter average surface roughness (Ra) can be misleading, and more work is required to establish a concrete correlation between surface topography and bacterial adhesion. It was highlighted that the two-dimensional Ra parameter is insufficient for describing the surface topography. The introduction of 3D surface characterization parameters is necessary to provide a richer set of surface descriptors. It is anticipated that this could provide a correlation with bactericidal effects. The challenge remains in the creation of these special hierarchical structured surfaces. Some of these structured surfaces require manipulation at multiple length scales and combining different scales on the same surface remains the most ambitious challenge in the manufacturing process.

This review highlighted the growing need for identifying materials and manufacturing solutions for scalable fabrication of patterned hierarchical structures that are demonstrated to be bactericidal. Production of nature-inspired nanostructured surfaces exhibiting dimensions of the order of a few nanometers (this limit is set by the size of the bacteria $\sim$ typically about 1 to 2 μm diameter for staphylococci) on the complex freeform medical implant materials is proposed to be a major 21st-century challenge as it involves multidisciplinary efforts ranging from manufacturing, materials, surface science, and biology disciplines to name a few.

Currently available commercial medical implants do not have the functionalities required to offset the formation of the biofilm that contributes to the infection. The cost-laden repeated surgeries, as a result, directly contribute to a significant cost burden on the national economy in a growing ageing society. This review shows that nature is a good inspiration to capture nanostructures that have resulted in many millennia of evolution, and their integration into new generations of products, vis-à-vis hierarchical structures is the key to achieve bactericidal surfaces. The most efficient and promising bactericidal surfaces were reviewed, and dragonfly wings or cicada wings were found to be exceptionally well-suited examples.

It was concluded that the topography, wettability, and chemistry of the surface are the critical aspects to consider in achieving the bactericidal surfaces, and the slope presented by these surfaces can allow machine learning to design functional surfaces hitherto not known to provide unique functionality.

Besides bactericidal surfaces, various ultra-precision manufacturing and metrology routes are reviewed in great length with a focus on using these methods for fabricating bactericidal surfaces in a scalable way. Femtosecond laser machining here appears as the possible solution for the futuristic products. It was finally concluded that to mimic

precisely natural surfaces, the ultra-precision manufacturing society needs to develop a radically new concept to produce scalable fabrication routes for the nature-inspired surfaces, and this journey seems to go via the path of "Precision additive manufacturing" (PAM), a technology that has yet to be fully developed but holds the key to the future of ultra-precision manufacturing.

DATA AVAILABILITY

All data in the manuscript will be available through the Cranfield University open repository 10.17862/cranfield.rd.12925706

REFERENCES

[1] S. Goel, S. Hawi, G. Goel, V. K. Thakur, A. Agrawal, C. Hoskins, O. Pearce, T. Hussain, H. M. Upadhyaya, G. Cross, and A. H. Barber, Mater. Today Chem. 17, 100300 (2020).

[2] D. Adamovic, B. Ristic, and F. Zivic, in Biomater. Clin. Pract. Adv. Clin. Res. Med. Devices (Springer International Publishing, 2017), pp. 47–99.

[3] W. F. Oliveira, P. M. S. Silva, R. C. S. Silva, G. M. M. Silva, G. Machado, L. C. B. B. Coelho, and M. T. S. Correia, J. Hosp. Infect. 98, 111 (2018).

[4] C. R. Arciola, D. Campoccia, and L. Montanaro, Nat. Rev. Microbiol. 16, 397 (2018).

[5] S. Veerachamy, T. Yarlagadda, G. Manivasagam, and P. K. Yarlagadda, Proc. Inst. Mech. Eng. Part H J. Eng. Med. 228, 1083 (2014).

[6] J. W. Costerton, L. Montanaro, and C. R. Arciola, Int. J. Artif. Organs 28, 1062 (2005).

[7] (n.d.).

[8] Y. Kirmanidou, M. Sidira, M. E. Drosou, V. Bennani, A. Bakopoulou, A. Tsouknidas, N. Michailidis, and K. Michalakis, BioMed Res. Int. 2016, 1.

[9] X. Liu, P. K. Chu, and C. Ding, Mater. Sci. Eng. R Rep. 47, 49 (2004).

[10] A. Tripathy, P. Sen, B. Su, and W. H. Briscoe, Adv. Colloid Interface Sci. 248, 85 (2017).

[11] L. Feng, S. Li, Y. Li, H. Li, L. Zhang, J. Zhai, Y. Song, B. Liu, L. Jiang, and D. Zhu, Adv. Mater. 14, 1857 (2002).

[12] G. S. Watson, D. W. Green, L. Schwarzkopf, X. Li, B. W. Cribb, S. Myhra, and J. A. Watson, Acta Biomater. 21, 109 (2015).

[13] B. Bhushan and Y. C. Jung, Prog. Mater. Sci. 56(1), 1 (2011).

[14] X. Zhang, L. Wang, and E. Levänen, RSC Adv. 3, 12003 (2013).

[15] C. D. Bandara, S. Singh, I. O. Afara, A. Wolff, T. Tesfamichael, K. Ostrikov, and A. Oloyede, ACS Appl. Mater. Interfaces 9, 6746 (2017).

[16] A. T. Poortinga, R. Bos, W. Norde, and H. J. Busscher, Surf. Sci. Rep. 47, 1–32 (2002).

[17] M. Hermansson, Colloids Surf. B Biointerfaces 14, 105–119 (1999).

[18] C. Desrousseaux, V. Sautou, S. Descamps, and O. Traoré, J. Hosp. Infect. 85, 87 (2013).

[19] E. O'Neill, C. Pozzi, P. Houston, H. Humphreys, D. A. Robinson, A. Loughman, T. J. Foster, and J. P. O'Gara, J. Bacteriol. 190, 3835 (2008).

[20] C. Berne, A. Ducret, G. G. Hardy, and, and Y. V. Brun, In Microb. Biofilms (ASM Press, Washington, DC, 2015), pp. 163–199.

[21] R. M. Donlan, in Emerging Infectious Diseases (Centers for Disease Control and Prevention, 2001), pp. 277–281.

[22] D. Lindsay and A. von Holy, J. Hosp. Infect. 64, 313 (2006).

[23] S. C. Cortelli, J. R. Cortelli, R. L. Romeiro, F. O. Costa, D. R. Aquino, P. R. Orzechowski, V. C. Araújo, and P. M. Duarte, Arch. Oral Biol. 58, 67 (2013).

[24] R. Wasfi, S. M. Hamed, M. A. Amer, and L. I. Fahmy, Front. Cell. Infect. Microbiol. 10, 414 (2020).

[25] H. Anwar, M. K. Dasgupta, and J. W. Costerton, Antimicrob. Agents Chemother. 34, 2043 (1990).

[26] K. L. Mittal, Contact Angle, Wettability and Adhesion, 5 (CRC Press, 2008).

[27] A. Cunha, Multiscale Femtosecond Laser Surface Texturing of Titanium and Titanium Alloys for Dental and Medical Orthopaedic Implants (Bordeaux, 2015).

[28] T. Sun, L. Feng, X. Gao, and L. Jiang, Acc. Chem. Res. 38, 644 (2005).

[29] K. Koch, B. Bhushan, and W. Barthlott, Prog. Mater. Sci. 54, 137 (2009).

[30] K. Koch, B. Bhushan, and W. Barthlott, Soft Matter 4, 1943 (2008).

[31] A. Malshe, K. Rajurkar, A. Samant, H. N. Hansen, S. Bapat, and W. Jiang, CIRP Ann. 62, 607 (2013).

[32] J. Genzer and K. Efimenko, Biofouling 22, 339 (2006).

[33] A. Marmur, Biofouling 22, 107 (2006).

[34] A. B. D. Cassie and S. Baxter, Trans. Faraday Soc. 40, 546 (1944).

[35] D. Patel, V. Jain, and J. Ramkumar, Proc. Inst. Mech. Eng. Part B J. Eng. Manuf. 232, 941 (2018).

[36] G. Carbone and L. Mangialardi, Eur. Phys. J. E 16, 67 (2005).

[37] J. Sun and B. Bhushan, Tribol. Int. 129, 67 (2019).

[38] J. Hasan, R. J. Crawford, and E. P. Ivanova, Trends Biotechnol. 31, 295 (2013).

[39] S. Nishimoto and B. Bhushan, RSC Adv. 3, 671 (2013).

[40] W. Barthlott and C. Neinhuis, Planta 202, 1 (1997).

[41] P. Y. Chen, J. McKittrick, and M. A. Meyers, Prog. Mater. Sci. 57, 1492 (2012).

[42] K. Koch, B. Bhushan, Y. C. Jung, and W. Barthlott, Soft Matter 5, 1386 (2009).

[43] H. J. Ensikat, P. Ditsche-Kuru, C. Neinhuis, and W. Barthlott, Beilstein J. Nanotechnol. 2, 152 (2011).

[44] B. Bhushan, Philos. Trans. R. Soc. A Math. Phys. Eng. Sci. 367, 1445 (2009).

[45] A. Jaggessar, H. Shahali, A. Mathew, and P. K. D. V. Yarlagadda, J. Nanobiotechnology 15, 64 (2017).

[46] E. Fadeeva, V. K. Truong, M. Stiesch, B. N. Chichkov, R. J. Crawford, J. Wang, and E. P. Ivanova, Langmuir 27, 3012 (2011).

[47] Y. Y. Yan, N. Gao, and W. Barthlott, Adv. Colloid Interface Sci. 169, 80 (2011).

[48] L. P. Biró, Mater. Sci. Eng. B Solid-State Mater. Adv. Technol. 169, 3 (2010).

[49] V. Saranathan, C. O. Osuji, S. G. J. Mochrie, H. Noh, S. Narayanan, A. Sandy, E. R. Dufresne, and R. O. Prum, Proc. Natl. Acad. Sci. 107, 11676 (2010).

[50] P. Vukusic, J. R. Sambles, C. R. Lawrence, and R. J. Wootton, Proc. R. Soc. London. Ser. B Biol. Sci. 266, 1403 (1999).

[51] Y. Ding, S. Xu, and Z. L. Wang, J. Appl. Phys. 106, 074702 (2009).

[52]S. Yoshioka and S. Kinoshita, Proc. R. Soc. London. Ser. B Biol. Sci. **271**, 581 (2004).

[53]Y. Zheng, X. Gao, and L. Jiang, Soft Matter **3**, 178 (2007).

[54]D. Y. Zhao, Z. P. Huang, M. J. Wang, T. Wang, and Y. Jin, J. Mater. Process. Technol. **212**, 198 (2012).

[55]K. K. Chung, J. F. Schumacher, E. M. Sampson, R. A. Burne, P. J. Antonelli, and A. B. Brennan, Biointerphases **2**, 89 (2007).

[56]J. F. Schumacher, M. L. Carman, T. G. Estes, A. W. Feinberg, L. H. Wilson, M. E. Callow, J. A. Callow, J. A. Finlay, and A. B. Brennan, Biofouling **23**, 55 (2007).

[57]J. F. Schumacher, N. Aldred, M. E. Callow, J. A. Finlay, J. A. Callow, A. S. Clare, and A. B. Brennan, Biofouling **23**, 307 (2007).

[58]V. Tinnemann, L. Hernández, S. C. L. Fischer, E. Arzt, R. Bennewitz, and R. Hensel, Adv. Funct. Mater. **29**, 1807713 (2019).

[59]B. Bhushan, J. Adhes. Sci. Technol. **21**, 1213 (2007).

[60]W. R. Hansen and K. Autumn, Proc. Natl. Acad. Sci. **102**, 385 (2005).

[61]K. Autumn, Y. A. Liang, S. T. Hsieh, W. Zesch, W. P. Chan, T. W. Kenny, R. Fearing, and R. J. Full, Nature **405**, 681 (2000).

[62]X. Li, G. S. Cheung, G. S. Watson, J. A. Watson, S. Lin, L. Schwarzkopf, and D. W. Green, Nanoscale **8**, 18860 (2016).

[63]E. P. Ivanova, J. Hasan, H. K. Webb, V. K. Truong, G. S. Watson, J. A. Watson, V. A. Baulin, S. Pogodin, J. Y. Wang, M. J. Tobin, C. Löbbe, and R. J. Crawford, Small **8**, 2489 (2012).

[64]G. S. Watson, S. Myhra, B. W. Cribb, and J. A. Watson, Biophys. J. **94**, 3352 (2008).

[65]J. Hasan, H. K. Webb, V. K. Truong, S. Pogodin, V. A. Baulin, G. S. Watson, J. A. Watson, R. J. Crawford, and E. P. Ivanova, Appl. Microbiol. Biotechnol. **97**, 9257 (2013).

[66]S. Pogodin, J. Hasan, V. A. Baulin, H. K. Webb, V. K. Truong, T. H. Phong Nguyen, V. Boshkovikj, C. J. Fluke, G. S. Watson, J. A. Watson, R. J. Crawford, and E. P. Ivanova, Biophys. J. **104**, 835 (2013).

[67]J. Román-Kustas, J. B. Hoffman, J. H. Reed, A. E. Gonsalves, J. Oh, L. Li, S. Hong, K. D. Jo, C. E. Dana, N. Miljkovic, D. M. Cropek, and M. Alleyne, Adv. Mater. Interfaces **7**, 2000112 (2020).

[68]D. E. Mainwaring, S. H. Nguyen, H. Webb, T. Jakubov, M. Tobin, R. N. Lamb, A. H. F. Wu, R. Marchant, R. J. Crawford, and E. P. Ivanova, Nanoscale **8**, 6527 (2016).

[69]C. M. Bhadra, V. Khanh Truong, V. T. H. Pham, M. Al Kobaisi, G. Seniutinas, J. Y. Wang, S. Juodkazis, R. J. Crawford, and E. P. Ivanova, Sci. Rep. **5**, 16817 (2015).

[70]K. Modaresifar, S. Azizian, M. Ganjian, L. E. Fratila-Apachitei, and A. A. Zadpoor, Acta Biomater. **83**, 29 (2019).

[71]A. A. Voevodin and J. S. Zabinski, Thin Solid Films **370**, 223 (2000).

[72]J. Teyssier, S. V. Saenko, D. Van Der Marel, and M. C. Milinkovitch, Nat. Commun. **6**, 6368 (2015).

[73]M. Spinner, G. Westhoff, and S. N. Gorb, Sci. Rep. **4**, 1 (2014).

[74]H. H. Chou, A. Nguyen, A. Chortos, J. W. F. To, C. Lu, J. Mei, T. Kurosawa, W. G. Bae, J. B. H. Tok, and Z. Bao, Nat. Commun. **6**, 1 (2015).

[75]M. Vatankhah-Varnosfaderani, A. N. Keith, Y. Cong, H. Liang, M. Rosenthal, M. Sztucki, C. Clair, S. Magonov, D. A. Ivanov, A. V. Dobrynin, and S. S. Sheiko, Science **359**, 1509 (2018).

[76]K. B. Karsten, G. W. Ferguson, T. Chen, and M. F. Holick, Physiol. Biochem. Zool. **82**, 218 (2009).

[77]H. Toyota, K. Takahara, M. Okano, T. Yotsuya, and H. Kikuta, Japanese J. Appl. Phys. **40**, L747 (2001).

[78]J. Aizenberg, A. Tkachenko, S. Weiner, L. Addadi, and G. Hendler, Nature **412**, 819 (2001).

[79]P. B. Applewhite, Behav. Biol. **7**, 47 (1972).

[80]H. S. Patil and S. Vaijapurkar, J. Bionic Eng. **4**, 19 (2007).

[81]M. Ueda, H. Shigemori, N. Sata, and S. Yamamura, Phytochemistry **53**, 39 (2000).

[82]H. Lowenstam and S. Weiner, *On Biomineralization* (Oxford University Press, 1989).

[83]D. R. Talham, Cryst. Growth Des. **2**, 675 (2002).

[84]J. Moradian-Oldak, H. B. Wen, G. B. Schneider, and C. M. Stanford, Periodontol. 2000 **41**, 157 (2006).

[85]P. Lucas, P. Constantino, B. Wood, and B. Lawn, BioEssays **30**, 374 (2008).

[86]P. Vukusic and J. R. Sambles, Nature **424**, 852 (2003).

[87]A. Ingram and A. Parker, Philos. Trans. R. Soc. B Biol. Sci. **363**, 2465 (2008).

[88]S. Kinoshita and S. Yoshioka, ChemPhysChem **6**, 1442 (2005).

[89]P. Vukusic and I. Hooper, Science **310**, 1151 (2005).

[90]S. C. Burgess, A. King, and R. Hyde, Opt. Laser Technol. **38**, 329 (2006).

[91]J. Zi, X. Yu, Y. Li, X. Hu, C. Xu, X. Wang, X. Liu, and R. Fu, Proc. Natl. Acad. Sci. **100**, 12576 (2003).

[92]L. D'Alba, V. Saranathan, J. A. Clarke, J. A. Vinther, R. O. Prum, and M. D. Shawkey, Biol. Lett. **7**, 543 (2011).

[93]G. S. Watson, D. W. Green, B. W. Cribb, C. L. Brown, C. R. Meritt, M. J. Tobin, J. Vongsvivut, M. Sun, A. P. Liang, and J. A. Watson, ACS Appl. Mater. Interfaces **9**, 24381 (2017).

[94]X. Pu, G. Li, and Y. Liu, ChemBioEng Rev. **3**, 26 (2016).

[95]D. W. Green, K. K. H. Lee, J. A. Watson, H. Y. Kim, K. S. Yoon, E. J. Kim, J. M. Lee, G. S. Watson, and H. S. Jung, Sci. Rep. **7**, 41023 (2017).

[96]G. S. Watson, J. A. Watson, S. Hu, C. L. Brown, B. W. Cribb, and S. Myhra, Int. J. Nanomanuf. **5**, 112 (2010).

[97]E. P. Ivanova, J. Hasan, H. K. Webb, G. Gervinskas, S. Juodkazis, V. K. Truong, A. H. F. Wu, R. N. Lamb, V. A. Baulin, G. S. Watson, J. A. Watson, D. E. Mainwaring, and R. J. Crawford, Nat. Commun. **4**, 2838 (2013).

[98]R. Selvakumar, K. K. Karuppanan, and R. Pezhinkattil, Micron **43**, 1299 (2012).

[99]J. Hasan, S. Raj, L. Yadav, and K. Chatterjee, RSC Adv. **5**, 44953 (2015).

[100]T. Diu, N. Faruqui, T. Sjöström, B. Lamarre, H. F. Jenkinson, B. Su, and M. G. Ryadnov, "Cicada-inspired cell-instructive nanopatterned arrays," Sci. Rep. **4**, 7122 (2014).

[101]C. Sengstock, M. Lopian, Y. Motemani, A. Borgmann, C. Khare, P. J. S. Buenconsejo, T. A. Schildhauer, A. Ludwig, and M. Köller, Nanotechnology **25**, 195101 (2014).

[102]G. Zhang, J. Zhang, G. Xie, Z. Liu, and H. Shao, Small **2**, 1440 (2006).

[103]T. Sjöström, A. H. Nobbs, and B. Su, Mater. Lett. **167**, 22 (2016).

[104]V. K. Truong, H. K. Webb, E. Fadeeva, B. N. Chichkov, A. H. F. Wu, R. Lamb, J. Y. Wang, R. J. Crawford, and E. P. Ivanova, Biofouling **28**, 539 (2012).

[105]A. Sakamoto, Y. Terui, C. Horie, T. Fukui, T. Masuzawa, S. Sugawara, K. Shigeta, T. Shigeta, K. Igarashi, and K. Kashiwagi, FEMS Microbiol. Lett. **361**, 10 (2014).

[106]D. W. Bechert, M. Bruse, and W. Hage, Exp. Fluids **28**, 403 (2000).

[107]E. E. Mann, M. R. Mettetal, R. M. May, M. C. Drinker, B. C. Stevenson, V. L. Baiamonte, J. M. Marso, E. A. Dannemiller, A. E. Parker, and S. T. Reddy, J. Microbiol. Exp. **1**, 32 (2014).

[108]Y. Wu, J. P. Zitelli, K. S. TenHuisen, X. Yu, and M. R. Libera, Biomaterials **32**, 951 (2011).

[109]V. K. Truong, R. Lapovok, Y. S. Estrin, S. Rundell, J. Y. Wang, C. J. Fluke, R. J. Crawford, and E. P. Ivanova, Biomaterials **31**, 3674 (2010).

[110]E. P. Ivanova, V. K. Truong, H. K. Webb, V. A. Baulin, J. Y. Wang, N. Mohammodi, F. Wang, C. Fluke, and R. J. Crawford, Sci. Rep. **1**, 1 (2011).

[111]F. Aykent, I. Yondem, A. G. Ozyesil, S. K. Gunal, M. C. Avunduk, and S. Ozkan, J. Prosthet. Dent. **103**, 221 (2010).

[112]R. L. Taylor, J. Verran, G. C. Lees, and A. J. P. Ward, J. Mater. Sci. Mater. Med. **9**, 17 (1998).

[113]E. W. McAllister, L. C. Carey, P. G. Brady, R. Heller, and S. G. Kovacs, Gastrointest. Endosc. **39**, 422 (1993).

[114]L. Baker and A. S. Greenham, J. Bone Joint Surg. Am. **7**, 1551 (1988).

[115]L. R. Hilbert, D. Bagge-Ravn, J. Kold, and L. Gram, Int. Biodeterior. Biodegrad. **52**, 175 (2003).

[116]I. Yoda, H. Koseki, M. Tomita, T. Shida, H. Horiuchi, H. Sakoda, and M. Osaki, BMC Microbiol. **14**, 234 (2014).

[117]R. J. Crawford, H. K. Webb, V. K. Truong, J. Hasan, and E. P. Ivanova, Adv. Colloid Interface Sci **179–182**, 142 (2012).

[118]A. Zabala, L. Blunt, W. Tato, A. Aginagalde, X. Gomez, and I. Llavori, in *MATEC Web Conf.* (EDP Sciences, 2018), p. 14013.

[119]B. Ercan, E. Taylor, E. Alpaslan, and T. J. Webster, Nanotechnology **22**, 295102 (2011).

[120]W.-Q. Yu, X.-Q. Jiang, L. Xu, Y.-F. Zhao, F.-Q. Zhang, and X. Cao, J. Biomed. Mater. Res. Part B Appl. Biomater. **99B**, 207 (2011).

[121]A. I. Hochbaum and J. Aizenberg, Nano Lett. **10**, 3717 (2010).

[122]M. Lorenzetti, I. Dogša, T. Stošicki, D. Stopar, M. Kalin, S. Kobe, and S. Novak, ACS Appl. Mater. Interfaces **7**, 1644 (2015).

[123]K. Anselme, P. Davidson, A. M. Popa, M. Giazzon, M. Liley, and L. Ploux, Acta Biomater. **6**, 3824 (2010).

[124]S. Wu, F. Zuber, K. Maniura-Weber, J. Brugger, and Q. Ren, J. Nanobiotechnology **16**, 1 (2018).

[125]X. Li and T. Chen, Phys. Rev. E **93**, 052419 (2016).

[126]A. Cunha, A. M. Elie, L. Plawinski, A. P. Serro, A. M. Botelho Do Rego, A. Almeida, M. C. Urdaci, M. C. Durrieu, and R. Vilar, Appl. Surf. Sci. **360**, 485 (2016).

[127]C. W. Chan, L. Carson, G. C. Smith, A. Morelli, and S. Lee, Appl. Surf. Sci. **404**, 67 (2017).

[128]Y. H. An and R. J. Friedman, J. Biomed. Mater. Res. **43**, 338 (1998).

[129]S. D. Puckett, E. Taylor, T. Raimondo, and T. J. Webster, Biomaterials **31**, 706 (2010).

[130]L. G. Harris and R. G. Richards, Injury **37**, S3 (2006).

[131]P. Tang, W. Zhang, Y. Wang, B. Zhang, H. Wang, C. Lin, and L. Zhang, "Effect of superhydrophobic surface of titanium on staphylococcus aureus adhesion," J. Nanomater. **2011**, 178921.

[132]J. H. Lee, G. Khang, J. W. Lee, and H. B. Lee, J. Colloid Interface Sci. **205**, 323 (1998).

[133]H. Yang and Y. Deng, J. Colloid Interface Sci. **325**, 588 (2008).

[134]D. Campoccia, L. Montanaro, H. Agheli, D. S. Sutherland, V. Pirini, M. E. Donati, and C. R. Arciola, Int. J. Artif. Organs **29**, 622 (2006).

[135]L. Visai, L. de Nardo, C. Punta, L. Melone, A. Cigada, M. Imbriani, and C. R. Arciola, Int. J. Artif. Organs **34**, 929 (2011).

[136]B. Del Curto, M. F. Brunella, C. Giordano, M. P. Pedeferri, V. Valtulina, L. Visai, and A. Cigada, Int. J. Artif. Organs **28**, 718 (2005).

[137]C. Giordano, E. Saino, L. Rimondini, M. P. Pedeferri, L. Visai, A. Cigada, and R. Chiesa, Colloids Surf. B Biointerfaces **88**, 648 (2011).

[138]C. C. Chu and D. F. Williams, Am. J. Surg. **147**, 197 (1984).

[139]M. J. Hajipour, K. M. Fromm, A. Akbar Ashkarran, D. Jimenez de Aberasturi, I. R. de Larramendi, T. Rojo, V. Serpooshan, W. J. Parak, and M. Mahmoudi, Trends Biotechnol. **30**, 499 (2012).

[140]S. Y. Liau, D. C. Read, W. J. Pugh, J. R. Furr, and A. D. Russell, Lett. Appl. Microbiol. **25**, 279 (1997).

[141]J. R. Morones, J. L. Elechiguerra, A. Camacho, K. Holt, J. B. Kouri, J. T. Ramírez, and M. J. Yacaman, Nanotechnology **16**, 2346 (2005).

[142]I. Sondi and B. Salopek-Sondi, J. Colloid Interface Sci. **275**, 177 (2004).

[143]X. H. N. Xu, W. J. Brownlow, S. V. Kyriacou, Q. Wan, and J. J. Viola, Biochemistry **43**, 10400 (2004).

[144]G. Borkow and J. Gabbay, Curr. Chem. Biol **3**, 272 (2009).

[145]A. K. Chatterjee, R. Chakraborty, and T. Basu, Nanotechnology **25**, 135101 (2014).

[146]L. F. Espinosa-Cristóbal, G. A. Martínez-Castañón, R. E. Martínez-Martínez, J. P. Loyola-Rodríguez, N. Patiño-Marín, J. F. Reyes-Macías, and F. Ruiz, Mater. Lett. **63**, 2603 (2009).

[147]L. Juan, Z. Zhimin, M. Anchun, L. Lei, and Z. Jingchao, Int. J. Nanomedicine **5**, 261 (2010).

[148]L. Zhao, H. Wang, K. Huo, L. Cui, W. Zhang, H. Ni, Y. Zhang, Z. Wu, and P. K. Chu, Biomaterials **32**, 5706 (2011).

[149]A. Mo, J. Liao, W. Xu, S. Xian, Y. Li, and S. Bai, Appl. Surf. Sci. **255**, 435 (2008).

[150]R. Sinha, R. Karan, A. Sinha, and S. K. Khare, Bioresour. Technol. **102**, 1516 (2011).

[151]S. Parham, D. H. B. Wicaksono, S. Bagherbaigi, S. L. Lee, and H. Nur, J. Chin. Chem. Soc. **63**, 385 (2016).

[152]Y. N. Slavin, J. Asnis, U. O. Häfeli, and H. Bach, J. Nanobiotechnology **15**, 65 (2017).

[153]S. M. Dizaj, F. Lotfipour, M. Barzegar-Jalali, M. H. Zarrintan, and K. Adibkia, Mater. Sci. Eng. C **44**, 278 (2014).

[154]S. Stankic, S. Suman, F. Haque, and J. Vidic, J. Nanobiotechnology **14**, 73 (2016).

[155]H. Qin, H. Cao, Y. Zhao, G. Jin, M. Cheng, J. Wang, Y. Jiang, Z. An, X. Zhang, and X. Liu, ACS Appl. Mater. Interfaces **7**, 10785 (2015).

[156]S. Mei, H. Wang, W. Wang, L. Tong, H. Pan, C. Ruan, Q. Ma, M. Liu, H. Yang, L. Zhang, Y. Cheng, Y. Zhang, L. Zhao, and P. K. Chu, Biomaterials **35**, 4255 (2014).

[157]Y. Zheng, J. Li, X. Liu, and J. Sun, Int. J. Nanomedicine **7**, 875 (2012).

[158]T. Zdziech, M. Hajduga, and D. Jedrzejczyk, in *Met. 2012 - Conf. Proceedings, 21st Int. Conf. Metall. Mater.* (2012).

[159]Y. Zhu, H. Cao, S. Qiao, M. Wang, Y. Gu, H. Luo, F. Meng, X. Liu, and H. Lai, Int. J. Nanomedicine **10**, 6659 (2015).

[160]G. Jin, H. Qin, H. Cao, S. Qian, Y. Zhao, X. Peng, X. Zhang, X. Liu, and P. K. Chu, Biomaterials **35**, 7699 (2014).

[161]H. Cao, W. Zhang, F. Meng, J. Guo, D. Wang, S. Qian, X. Jiang, X. Liu, and P. K. Chu, ACS Appl. Mater. Interfaces **9**, 5149 (2017).

[162]I. Lampé, D. Beke, S. Biri, I. Csarnovics, A. Csik, Z. Dombrádi, P. Hajdu, V. Hegedűs, R. Rácz, I. Varga, and C. Hegedűs, Int. J. Nanomedicine **14**, 4709 (2019).

[163]G. Wang, W. Jin, A. M. Qasim, A. Gao, X. Peng, W. Li, H. Feng, and P. K. Chu, Biomaterials **124**, 25 (2017).

[164]C. Zhu, N. R. Bao, S. Chen, and J. N. Zhao, Appl. Surf. Sci. **389**, 7 (2016).

[165]X. Hou, D. Mao, H. Ma, Y. Ai, X. Zhao, J. Deng, D. Li, and B. Liao, Mater. Lett. **161**, 309 (2015).

[166]X. Hou, H. Ma, F. Liu, J. Deng, Y. Ai, X. Zhao, D. Mao, D. Li, and B. Liao, J. Hazard. Mater. **299**, 59 (2015).

[167]S. Qiao, H. Cao, X. Zhao, H. Lo, L. Zhuang, Y. Gu, J. Shi, X. Liu, and H. Lai, Int. J. Nanomedicine **10**, 653 (2015).

[168]J. Osés, J. F. Palacio, S. Kulkarni, A. Medrano, J. A. García, and R. Rodríguez, Appl. Surf. Sci. **310**, 56 (2014).

[169]P. Zhang, Z. Zhang, and W. Li, "Antibacterial TiO_2 coating incorporating silver nanoparticles by microarc oxidation and ion implantation," J. Nanomater. **2013**, 542878.

[170]R. Chen, H. Ni, H. Zhang, G. Yue, W. Zhan, and P. Xiong, Vacuum **89**, 249–253 (2013).

[171]H. Cao, X. Liu, F. Meng, and P. K. Chu, Biomaterials **32**, 693 (2011).

[172]J. Zhao, H. J. Feng, H. Q. Tang, and J. H. Zheng, "Bactericidal and corrosive properties of silver implanted TiN thin films coated on AISI317 stainless steel," Surf. Coat. Technol. **201**, 5676–5679 (2007).

[173]H. Q. Tang, T. Liu, X. Liu, H. Q. Gu, and J. Zhao, Nucl. Instrum. Methods Phys. Res. Sect. B Beam Interact. with Mater. Atoms **255**, 304 (2007).

[174]G. Jin, H. Qin, H. Cao, Y. Qiao, Y. Zhao, X. Peng, X. Zhang, X. Liu, and P. K. Chu, Biomaterials **65**, 22 (2015).

[175]H. Cao, T. Cui, G. Jin, and X. Liu, Surf. Coat. Technol. **256**, 9 (2014).

[176]R. Huang, Y. Han, and S. Lu, J. Mater. Chem. B **2**, 4531 (2014).

[177]H. W. Ni, H. S. Zhang, R. S. Chen, W. T. Zhan, K. F. Huo, and Z. Y. Zuo, Int. J. Miner. Metall. Mater. **19**, 4 (2012); available at https://link.springer.com/article/10.1007/s12613-012-0558-6.

[178]J. Fiedler, A. Kolitsch, B. Kleffner, D. Henke, S. Stenger, and R. E. Brenner, Int. J. Artif. Organs **34**, 882 (2011).

[179]W. Zhang and P. K. Chu, Surf. Coat. Technol. **203**, 909 (2008).

[180]Y. Z. Wan, S. Raman, F. He, and Y. Huang, Vacuum **81**, 1114 (2007).

[181]J. Vetter, Surf. Coat. Technol. **257**, 213 (2014).

[182]K. Bewilogua and D. Hofmann, Surf. Coat. Technol. **242**, 214 (2014).

[183]R. Hauert, K. Thorwarth, and G. Thorwarth, Surf. Coat. Technol. **233**, 119 (2013).

[184]J. Liu, D. A. Sonshine, S. Shervani, and R. H. Hurt, ACS Nano **4**, 6903 (2010).

[185]H. W. Choi, R. H. Dauskardt, S. C. Lee, K. R. Lee, and K. H. Oh, Diam. Relat. Mater. **17**, 252 (2008).

[186]K. Baba, R. Hatada, S. Flege, W. Ensinger, Y. Shibata, J. Nakashima, T. Sawase, and T. Morimura, Vacuum **89**, 179–184 (2013).

[187]W. C. Lan, S. F. Ou, M. H. Lin, K. L. Ou, and M. Y. Tsai, Ceram. Int. **39**, 4099 (2013).

[188]R. Hatada, S. Flege, A. Bobrich, W. Ensinger, C. Dietz, K. Baba, T. Sawase, T. Watamoto, and T. Matsutani, Appl. Surf. Sci. **310**, 257 (2014).

[189]M. Cloutier, R. Tolouei, O. Lesage, L. Lévesque, S. Turgeon, M. Tatoulian, and D. Mantovani, Biointerphases **9**, 029013 (2014).

[190]T. Juknius, M. Ružauskas, T. Tamulevičius, R. Šiugždinienė, I. Juknienė, A. Vasiliauskas, A. Jurkevičiūtė, and S. Tamulevičius, Materials **9**, 371 (2016).

[191]L. Swiatek, A. Olejnik, J. Grabarczyk, A. Jedrzejczak, A. Sobczyk-Guzenda, M. Kaminska, W. Jakubowski, W. Szymanski, and D. Bociaga, Diam. Relat. Mater. **67**, 54 (2016).

[192]G. Zakarienė, A. Novoslavskij, Š. Meškinis, A. Vasiliauskas, A. Tamulevičienė, S. Tamulevičius, T. Alter, and M. Malakauskas, Diam. Relat. Mater. **81**, 118 (2018).

[193] M. Janusz, L. Major, M. Kot, M. Dyner, J. M. Lackner, and B. Major, Biotribology **13**, 16 (2018).

[194] N. K. Manninen, S. V. Calderon, I. Carvalho, M. Henriques, A. Cavaleiro, and S. Carvalho, Appl. Surf. Sci. **377**, 283 (2016).

[195] L. J. Wang, F. Zhang, A. Fong, K. M. Lai, P. W. Shum, Z. F. Zhou, Z. F. Gao, and T. Fu, Thin Solid Films **650**, 58 (2018).

[196] A. Almaguer-Flore, S. E. Rodil, and R. Olivares-Navarrete, "Oral bacterial adhesion and biocompatibility of silver-amorphous carbon films; A surface modification for dental implants," in *Implant Dentistry,* edited by Ilser Turkyilmaz (IntechOpen, Rijeka, Croatia, 2011), 12.

[197] D. Bociaga, P. Komorowski, D. Batory, W. Szymanski, A. Olejnik, K. Jastrzebski, and W. Jakubowski, Appl. Surf. Sci. **355**, 388 (2015).

[198] D. Bociaga, W. Jakubowski, P. Komorowski, A. Sobczyk-Guzenda, A. Jędrzejczak, D. Batory, and A. Olejnik, Mater. Sci. Eng. C **63**, 462 (2016).

[199] F. P. Schwarz, I. Hauser-Gerspach, T. Waltimo, and B. Stritzker, Surf. Coat. Technol. **205**, 4850 (2011).

[200] N. Harrasser, S. Jüssen, I. J. Banke, R. Kmeth, R. von Eisenhart-Rothe, B. Stritzker, H. Gollwitzer, and R. Burgkart, AMB Express **5**, 77 (2015).

[201] C. Gorzelanny, R. Kmeth, A. Obermeier, A. T. Bauer, N. Halter, K. Kümpel, M. F. Schneider, A. Wixforth, H. Gollwitzer, R. Burgkart, B. Stritzker, and S. W. Schneider, Sci. Rep. **6**, 1 (2016).

[202] N. Harrasser, S. Jüssen, I. J. Banke, R. Kmeth, R. von Eisenhart-Rothe, B. Stritzker, H. Gollwitzer, and R. Burgkart, "Antibacterial efficacy of ultra-high molecular weight polyethylene with silver containing diamond-like surface layers," AMB Express **5**, 64 (2015).

[203] N. Harrasser, S. Jüssen, A. Obermeir, R. Kmeth, B. Stritzker, H. Gollwitzer, and R. Burgkart, Biomater. Res. **20**, 1 (2016).

[204] A. Mazare, A. Anghel, C. Surdu-Bob, G. Totea, I. Demetrescu, and D. Ionita, Thin Solid Films **657**, 16 (2018).

[205] F. R. Marciano, L. F. Bonetti, L. V. Santos, N. S. Da-Silva, E. J. Corat, and V. J. Trava-Airoldi, Diam. Relat. Mater. **18**, 1010 (2009).

[206] J. L. Endrino, M. Allen, R. E. Galindo, H. Zhang, A. Anders, and J. M. Albella, in *Mater. Res. Soc. Symp. Proc.* (Materials Research Society, 2006), pp. 105–111.

[207] J. L. Endrino, R. E. Galindo, H. S. Zhang, M. Allen, R. Gago, A. Espinosa, and A. Anders, Surf. Coat. Technol. **202**, 3675 (2008).

[208] J. L. Endrino, A. Anders, J. M. Albella, J. A. Horton, T. H. Horton, P. R. Ayyalasomayajula, and M. Allen, J. Phys. Conf. Ser. **252**, 012012 (2010).

[209] S. C. H. Kwok, W. Zhang, G. J. Wan, D. R. McKenzie, M. M. M. Bilek, and P. K. Chu, Diam. Relat. Mater. **16**, 1353 (2007).

[210] N. M. Chekan, N. M. Beliauski, V. V. Akulich, L. V. Pozdniak, E. K. Sergeeva, A. N. Chernov, V. V. Kazbanov, and V. A. Kulchitsky, Diam. Relat. Mater. **18**, 1006 (2009).

[211] R. J. Narayan, H. Wang, and A. Tiwari, in *Mater. Res. Soc. Symp. Proc.* (Materials Research Society, 2002), pp. 205–210.

[212] M. L. Morrison, R. A. Buchanan, P. K. Liaw, C. J. Berry, R. L. Brigmon, L. Riester, H. Abernathy, C. Jin, and R. J. Narayan, Diam. Relat. Mater. **15**, 138 (2006).

[213] I. N. Mihailescu, D. Bociaga, G. Socol, G. E. Stan, M. C. Chifiriuc, C. Bleotu, M. A. Husanu, G. Popescu-Pelin, L. Duta, C. R. Luculescu, I. Negut, C. Hapenciuc, C. Besleaga, I. Zgura, and F. Miculescu, Int. J. Pharm. **515**, 592 (2016).

[214] P. Písařík, M. Jelínek, J. Remsa, J. Mikšovský, J. Zemek, K. Jurek, S. Kubinová, J. Lukeš, and J. Šepitka, Mater. Sci. Eng. C **77**, 955 (2017).

[215] L. Duta, C. Ristoscu, G. E. Stan, M. A. Husanu, C. Besleaga, M. C. Chifiriuc, V. Lazar, C. Bleotu, F. Miculescu, N. Mihailescu, E. Axente, M. Badiceanu, D. Bociaga, and I. N. Mihailescu, Appl. Surf. Sci. **441**, 871 (2018).

[216] H. Morisaki and H. Tabuchi, Colloids Surf. B Biointerfaces **74**, 51 (2009).

[217] F. Hamadi, H. Latrache, M. Mabrrouki, A. Elghmari, A. Outzourhit, M. Ellouali, and A. Chtaini, J. Adhes. Sci. Technol. **19**, 73 (2005).

[218] T. R. Garrett, M. Bhakoo, and Z. Zhang, Prog. Nat. Sci. **18**, 1049 (2008).

[219] A. A. G. Bruzzone, H. L. Costa, P. M. Lonardo, and D. A. Lucca, CIRP Ann. **57**, 750 (2008).

[220] D. Mijatovic, J. C. T. Eijkel, and A. Van Den Berg, Lab Chip **5**, 492 (2005).

[221] A. Biswas, I. S. Bayer, A. S. Biris, T. Wang, E. Dervishi, and F. Faupel, Adv. Colloid Interface Sci. **170**, 2 (2012).

[222] S. Goel, M. Knaggs, G. Goel, X. W. Zhou, H. M. Upadhyaya, V. K. Thakur, V. Kumar, G. Bizarri, A. Tiwari, A. Murphy, A. Stukowski, and A. Matthews, Mater. Today Chem. **18**, 100356 (2020).

[223] K. Das, S. Bose, and A. Bandyopadhyay, Acta Biomater. **3**, 573 (2007).

[224] J. Gopal, R. P. George, P. Muraleedharan, and H. S. Khatak, Biofouling **20**, 167 (2004).

[225] B. Ercan, K. M. Kummer, K. M. Tarquinio, and T. J. Webster, Acta Biomater. **7**, 3003 (2011).

[226] A. Bendavid, P. J. Martin, L. Randeniya, and M. S. Amin, Diam. Relat. Mater. **18**, 66 (2009).

[227] O. Santos, T. Nylander, R. Rosmaninho, G. Rizzo, S. Yiantsios, N. Andritsos, A. Karabelas, H. Müller-Steinhagen, L. Melo, L. Boulangé-Petermann, C. Gabet, A. Braem, C. Trägårdh, and M. Paulsson, J. Food Eng. **64**, 63 (2004).

[228] Y.-Y. Zhao, B. Zhao, X. Su, S. Zhang, S. Wang, R. Keatch, and Q. Zhao, Biofouling **34**, 26 (2018).

[229] A. Ewald, S. K. Glückermann, R. Thull, and U. Gbureck, Biomed. Eng. Online **5**, 22 (2006).

[230] K. C. Park, H. J. Choi, C. H. Chang, R. E. Cohen, G. H. McKinley, and G. Barbastathis, ACS Nano **6**, 3789 (2012).

[231] T. R. Rautray, R. Narayanan, and K. H. Kim, Prog. Mater. Sci. **56**, 1137 (2011).

[232] *Titanium in Medicine*, edited by D. M. Brunette, P. Tengvall, M. Textor, and P. Thomsen (Springer, Berlin, 2001); available at https://www.springer.com/gp/book/9783642631191.

[233] J. Xu, G. Ding, J. Li, S. Yang, B. Fang, H. Sun, and Y. Zhou, Appl. Surf. Sci. **256**, 7540 (2010).

[234] S. Mändl, R. Sader, G. Thorwarth, D. Krause, H. F. Zeilhofer, H. H. Horch, and B. Rauschenbach, Biomol. Eng. **19**, 129 (2002).

[235] M. N. Dickson, E. I. Liang, L. A. Rodriguez, N. Vollereaux, and A. F. Yee, Biointerphases **10**, 021010 (2015).

[236] S. Wu, F. Zuber, J. Brugger, K. Maniura-Weber, and Q. Ren, Nanoscale **8**, 2620 (2016).

[237] L. G. Harris, S. Tosatti, M. Wieland, M. Textor, and R. G. Richards, Biomaterials **25**, 4135 (2004).

[238] W.-H. Kim, S.-B. Lee, K.-T. Oh, S.-K. Moon, K.-M. Kim, and K.-N. Kim, Surf. Interface Anal. **40**, 202 (2008).

[239] K. C. Popat, M. Eltgroth, T. J. LaTempa, C. A. Grimes, and T. A. Desai, Biomaterials **28**, 4880 (2007).

[240] C. R. Crick, S. Ismail, J. Pratten, and I. P. Parkin, Thin Solid Films **519**, 3722 (2011).

[241] L. Li, M. Hong, M. Schmidt, M. Zhong, A. Malshe, B. Huis In'Tveld, and V. Kovalenko, CIRP Ann. **60**, 735 (2011).

[242] J. Dutta Majumdar and I. Manna, Sadhana **28**, 495 (2003).

[243] T. N. Baker, in *Surface Engineering of Light Alloys: Aluminum, Magnesium, and Titanium Alloys.* (Woodhead, 2010).

[244] T. L. See, thesis, University of Manchester (2015).

[245] F. C. Burns and S. R. Cain, J. Phys. D. Appl. Phys. **29**, 1349 (1996).

[246] M. P. Fiorucci, A. J. López, and A. Ramil, Int. J. Adv. Manuf. Technol. **75**, 515 (2014).

[247] B. N. Chichkov, C. Momma, S. Nolte, F. von Alvensleben, and A. Tünnermann, Appl. Phys. A **63**, 109 (1996).

[248] H. Reimers, J. Gold, B. Kasemo, and D. Chakarov, Appl. Phys. A **77**, 491 (2003).

[249] F. J. C. Braga, R. F. C. Marques, E. de A. Filho, and A. C. Guastaldi, Appl. Surf. Sci. **253**, 9203 (2007).

[250] M. Trtica, B. Gakovic, D. Batani, T. Desai, P. Panjan, and B. Radak, Appl. Surf. Sci. **253**, 2551 (2006).

[251] B. K. Nayak, M. C. Gupta, and K. W. Kolasinski, Appl. Phys. A **90**, 399 (2008).

[252] W. O. Soboyejo, C. Mercer, S. Allameh, B. Nemetski, N. Marcantonio, and J. L. Ricci, Key Eng. Mater **198–199**, 203 (2001).

[253] S. Shaikh, S. Kedia, D. Singh, M. Subramanian, and S. Sinha, J. Laser Appl. **31**, 022011 (2019).

[254] J. Chen, S. Mwenifumbo, C. Langhammer, J.-P. McGovern, M. Li, A. Beye, and W. O. Soboyejo, J. Biomed. Mater. Res. Part B Appl. Biomater. **82B**, 360 (2007).

[255] A. Y. Fasasi, S. Mwenifumbo, N. Rahbar, J. Chen, M. Li, A. C. Beye, C. B. Arnold, and W. O. Soboyejo, Mater. Sci. Eng. C **29**, 5 (2009).

[256] A. C. Duncan, F. Weisbuch, F. Rouais, S. Lazare, and C. Baquey, Biosens. Bioelectron. **17**, 413 (2002).

[257]L. Giner, M. Mercadé, S. Torrent, M. Punset, R. A. Pérez, L. M. Delgado, and F. J. Gil, J. Appl. Biomater. Funct. Mater. **16**, 83 (2018).

[258]S. Zinelis, Dent. Mater. **23**, 601 (2007).

[259]A. K. Geim, S. V. Dubonos, I. V. Grigorieva, K. S. Novoselov, A. A. Zhukov, and S. Y. Shapoval, Nat. Mater. **2**, 461 (2003).

[260]S. Latthe, C. Terashima, K. Nakata, and A. Fujishima, Molecules **19**, 4256 (2014).

[261]D. Patil, S. Aravindan, M. K. Wasson, P. Vivekanandan, and P. V. Rao, J. Micro Nano-Manuf. **6**, 011002 (2018).

[262]R. Bürgers, T. Gerlach, S. Hahnel, F. Schwarz, G. Handel, and M. Gosau, Clin. Oral Implants Res. **21**, 156 (2010).

[263]F. Variola, S. F. Zalzal, A. Leduc, J. Barbeau, and A. Nanci, Int. J. Nanomedicine **9**, 2319 (2014).

[264]D. J. Balazs, K. Triandafillu, Y. Chevolot, B.-O. Aronsson, H. Harms, P. Descouts, and H. J. Mathieu, Surf. Interface Anal. **35**, 301 (2003).

[265]C. Serrano, L. García-Fernández, J. P. Fernández-Blázquez, M. Barbeck, S. Ghanaati, R. Unger, J. Kirkpatrick, E. Arzt, L. Funk, P. Turón, and A. del Campo, Biomaterials **52**, 291 (2015).

[266]B. Bhushan, *Springer Handbook of Nanotechnology*, 4th ed. (Springer, 2017).

[267]R. Jiang, L. Hao, L. Song, L. Tian, Y. Fan, J. Zhao, C. Liu, W. Ming, and L. Ren, Chem. Eng. J. **398**, 125609 (2020).

[268]X.-Q. Liu, Q.-D. Chen, R. Wang, L. Wang, X.-L. Yu, J.-N. Cao, Y.-M. Zhou, and H.-B. Sun, Adv. Mater. Interfaces **2**, 1500058 (2015).

[269]D. V. Ta, A. Dunn, T. J. Wasley, R. W. Kay, J. Stringer, P. J. Smith, C. Connaughton, and J. D. Shephard, Appl. Surf. Sci. **357**, 248 (2015).

[270]R. Leach, *Optical Measurement of Surface Topography* (Springer, 2011).

[271]*A Practical Guide to Surface Metrology* edited by M. Quinten (Springer, Berlin, 2019); available at https://www.springer.com/gp/book/9783030294533.

[272]H. Villarraga-Gómez, L. Körner, R. Leach, and S. T. Smith, "Amplitude-wavelength maps for X-ray computed tomography systems" Precis. Eng. **64**, 228–242 (2020).

[273]S. Rosén, T. R. Thomas, and B. G. Rosén, Surf. Topogr. Metrol. Prop **2**, 014005 (2013).

[274]K. Stout and L. Blunt, *Three Dimensional Surface Topography*, 2nd ed. (Elsevier, 2000).